Latitude dependence of Martian pedestal craters: Evidence for a sublimation-driven formation mechanism

Seth J. Kadish,[1] Nadine G. Barlow,[2] and James W. Head[1]

Received 13 December 2008; revised 31 March 2009; accepted 23 June 2009; published 1 October 2009.

[1] We report on the results of a survey to document and characterize pedestal craters on Mars equatorward of ~60°N and 65°S latitude. The identification of 2696 pedestal craters reveals a strong latitude dependence, with the vast majority found poleward of 33°N and 40°S. This latitudinal extent is correlated with many climate indicators consistent with the presence of an ice-rich substrate and with climate model predictions of where ice is deposited during periods of higher obliquity in the Amazonian. We have measured key physical attributes of pedestal craters, including the farthest radial extents of the pedestals, pedestal heights, and the circularity of the pedestal margins. In conjunction with the geographic distribution, our measurements strongly support a sublimation-related formation mechanism. This is in contrast to previous hypotheses, which have relied on eolian deflation to produce the elevated plateaus. The identification of marginal pits on the scarps of some pedestal craters, interpreted to be sublimation pits, provide direct evidence for the presence of ice-rich material underlying the armored surface of pedestal craters. On the basis of our findings, we propose a formation mechanism whereby projectiles impact into a volatile-rich dust/snow/ice substrate tens to hundreds of meters thick overlying a dominantly fragmental silicate regolith. The area surrounding the resulting crater becomes armored. Pedestals extend to a distance of multiple crater radii, farther than typical ejecta deposits, necessitating an armoring mechanism that is capable of indurating the surface to a distance greater than the reach of the ejecta. Return to low obliquity causes sublimation of the volatile-rich layer from the intercrater plains, lowering the elevation of the regional terrain. This yields generally circular pedestal craters elevated above the surrounding plains. As a result, the armored surfaces of pedestal craters have preserved a significant record of Amazonian climate history in the form of ice-rich deposits.

Citation: Kadish, S. J., N. G. Barlow, and J. W. Head (2009), Latitude dependence of Martian pedestal craters: Evidence for a sublimation-driven formation mechanism, *J. Geophys. Res.*, *114*, E10001, doi:10.1029/2008JE003318.

1. Introduction and Background

[2] Pedestal craters are a subclass of impact craters on Mars [*Barlow et al.*, 2000] characterized by a crater perched near the center of a pedestal (mesa or plateau) that is surrounded by an often circular, outward-facing scarp; the scarp is typically several crater diameters from the rim crest, and tens to over 100 m above the surrounding plains. First recognized in Mariner 9 data [*McCauley*, 1973], pedestal craters have been interpreted to form by armoring of the substrate during the impact event, usually by an ejecta covering [e.g., *Arvidson et al.*, 1976]. More recent hypotheses include increased ejecta mobilization caused by volatile substrates [*Osinski*, 2006], distal impact melt–rich veneers [*Schultz and Mustard*, 2004], and/or an atmospheric blast/thermal effect [*Wrobel et al.*, 2006]. Following armoring, a marginal scarp is created by preferential erosion of the substrate surrounding the armored region, historically thought to involve eolian deflation of the fine-grained, nonarmored, intercrater terrain [e.g., *McCauley*, 1973; *Arvidson et al.*, 1976, 1979]. This model, however, is not consistent with the commonly circular planform of pedestal craters; erosion via a predominant wind direction would likely produce asymmetric pedestals [e.g., *Head and Roth*, 1976; *Mutch and Woronow*, 1980; *Greeley et al.*, 2001]. Alternatively, the preferential distribution of pedestal craters at latitudes poleward of ~40° [*Mouginis-Mark*, 1979; *Kadish and Barlow*, 2006], in conjunction with an increased understanding of the role of redistributed ice and dust during periods of climate change [e.g., *Jakosky et al.*, 1995; *Head et al.*, 2003] have led many researchers to suspect that the substrate might have been volatile-rich [e.g., *Head and Roth*, 1976; *Mouginis-Mark*, 1987; *Schultz and Lutz*, 1988; *Barlow*, 2006; *Kadish and Barlow*, 2006; *Larson*, 2007]. Specifically, some [e.g., *Kadish and Barlow*, 2006] have called on models of impact into volatile-rich targets to

[1]Department of Geological Sciences, Brown University, Providence, Rhode Island, USA.
[2]Department of Physics and Astronomy, Northern Arizona University, Flagstaff, Arizona, USA.

0148-0227/09/2008JE003318

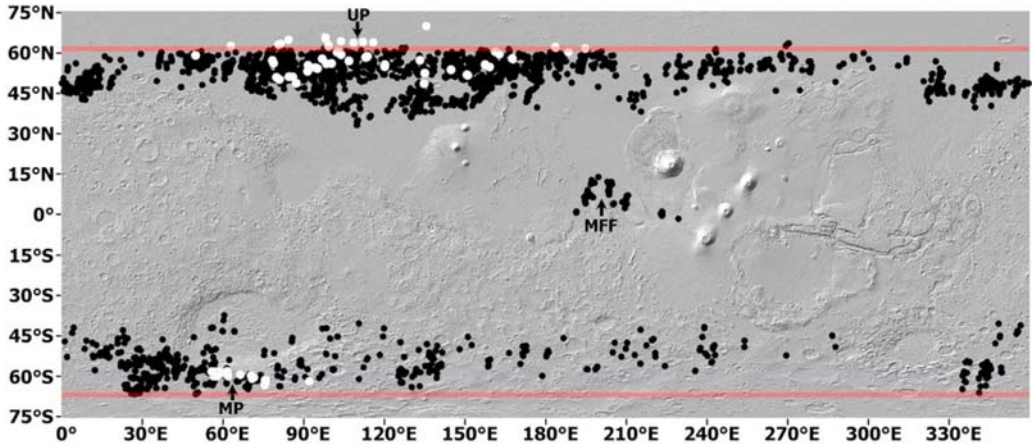

Figure 1. The geographic distribution of nonpitted pedestal craters (black circles) and pedestal craters with marginal pits (white circles) between ~60°N and 65°S on Mars. Pedestal craters with marginal pits were found in Utopia Planitia (UP) and Malea Planum (MP). The Medusae Fossae Formation (MFF) hosted the only population of equatorial pedestal craters.

produce pedestal craters during times of higher obliquity, when middle-latitude to high-latitude substrates are thought to have been characterized by thick deposits of snow and ice; return to lower obliquities would cause sublimation of the volatile-rich units, except below the protective cover of pedestal craters, and migration of the volatiles back to the poles [e.g., *Head et al.*, 2003; *Levrard et al.*, 2004]. Thus, this model predicts that thick deposits of snow and ice should underlie the armored pedestal crater surfaces.

[3] Here we report on the results of a comprehensive study using new image and altimetry data designed to document and characterize pedestal craters on Mars equatorward of ~60°N and 65°S latitude in order to test these hypotheses for the origin of pedestal craters. We identified 2696 pedestal craters between ~60°N and 65°S latitude; their distribution is strongly latitude-dependent, with the vast majority found poleward of 33°N and 40°S [*Kadish and Barlow*, 2006].

2. Methodology

[4] Pedestal craters were primarily identified through a survey of all Thermal Emission Imaging System (THEMIS) IR images, releases 1 through 23, between ~60°N and 65°S (Figures 1–4). This was supported in certain regions of interest by THEMIS VIS data; THEMIS VIS data were not used for the general survey owing to their limited coverage.

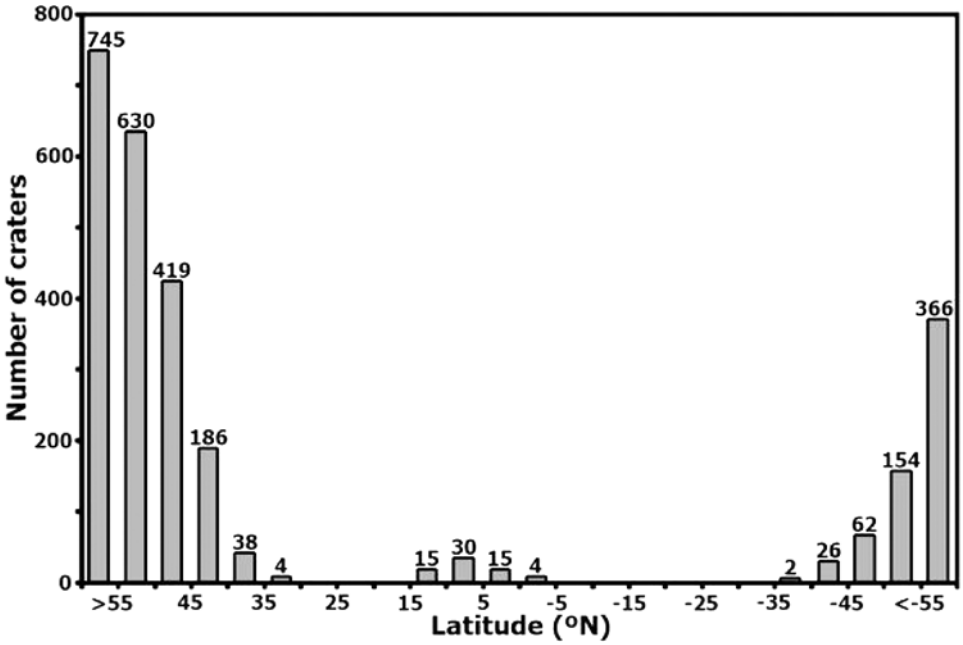

Figure 2. Histogram of the pedestal crater latitudinal distribution seen in Figure 1. The northern hemisphere has more than three times as many pedestal craters as the southern hemisphere over the latitudes surveyed. The number of pedestal craters increases as latitude increases. The values of craters/km^2, which account for changes in the areas of the latitudinal bands, are shown in Table 1.

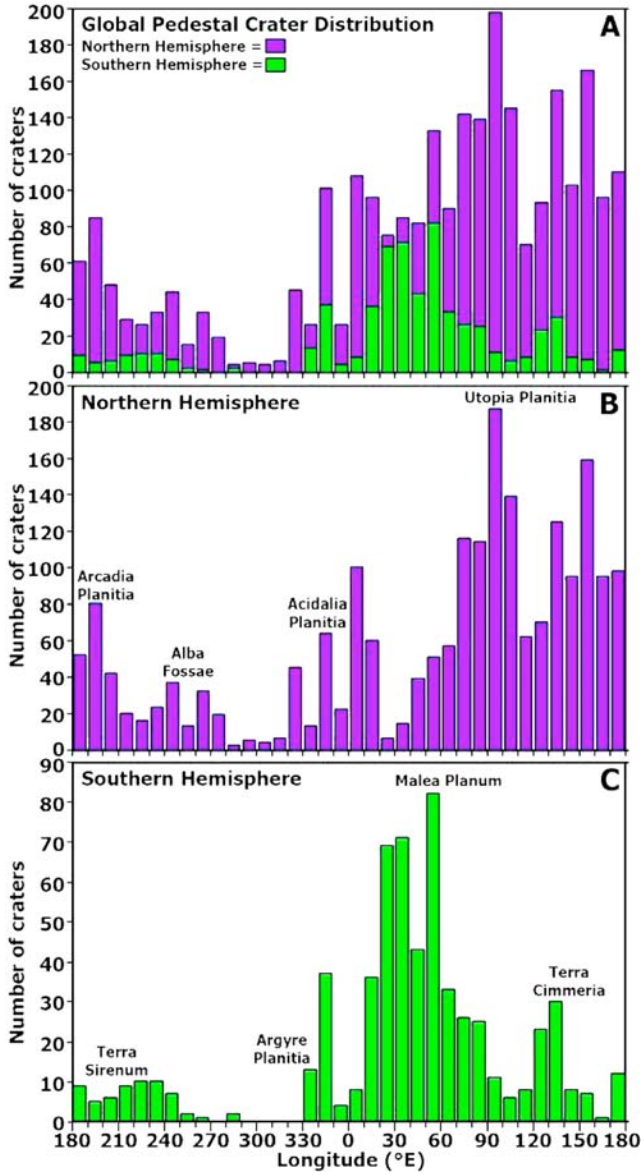

Figure 3. Histograms showing the longitudinal distribution of pedestal craters (a) globally, and within the (b) northern and (c) southern hemispheres. These emphasize the concentration of pedestal craters between 60° and 180°E in the northern hemisphere (Utopia Planitia) and between 0 and 120°E in the southern hemisphere (Malea Planum). There is a paucity of pedestal craters located in both hemispheres between 210° and 330°E.

Additionally, morphological assessments of specific pedestal craters utilized Mars Orbital Camera (MOC), High-Resolution Stereo Camera (HRSC), Context Camera (CTX), and High Resolution Imaging Science Experiment (HiRISE) data. Owing to the resolution of THEMIS IR images (100 m/pix) (Figure 4), pedestal craters <0.7 km in diameter were not analyzed. Although numerous pedestal craters are present poleward of 60° latitude, we selected this geographic range because we are particularly interested in how close to the equator pedestal craters are capable of forming; in order to test a sublimation-driven formation hypothesis, we wanted to compare the middle-latitude and low-latitude extent of pedestal craters to where we expect ice-rich material to have been emplaced during periods of high obliquity, on the basis of climate models and other ice-related morphologies. The study was expanded to 70°N and S for pedestal craters with marginal pits [*Kadish et al.*, 2008]. Measurements of pedestal craters, which included the crater diameter, farthest radial extent of the pedestal, and pedestal perimeter, were made using THEMIS IR data, and pedestal heights were derived from Mars Orbital Laser Altimeter (MOLA) data. These measurements allowed for the calculation of pedestal circularity (Γ) values (referred to previously in the literature as ''lobateness'' values) [*Kargel*, 1986; *Barlow*, 1994; *Barnouin-Jha and Schultz*, 1998] and pedestal to crater radius (P/C) ratios (referred to previously in the literature as ''ejecta mobility ratios'') [*Mouginis-Mark*, 1979; *Costard*, 1989; *Barlow*, 2004]. A Γ of 1 represents a perfectly circular pedestal, while higher values correspond to more sinuous/jagged perimeters. These dimensionless attributes are calculated by [*Barlow*, 2006]:

$$\Gamma = (\text{pedestal perimeter})/[4\pi(\text{pedestal area})]^{1/2} \quad (1)$$

$$\text{P/C ratio} = (\text{farthest extent of pedestal})/(\text{crater radius}) \quad (2)$$

3. Results

3.1. Distribution of Pedestal Craters

[5] Pedestal craters are not distributed randomly on Mars (Figures 1–3). In the northern hemisphere, pedestal craters are observed almost exclusively poleward of 33°N, with the majority between 45° and 60°N latitude (Figures 1 and 2 and Table 1), and between 70° and 180°E longitude (Figure 3). In the southern hemisphere, pedestal craters are less abundant (Figure 2), occurring almost exclusively poleward of 40°S latitude, between 10° and 90°E longitude (Figures 1 and 3). The highest concentrations occur in Utopia Planitia, east of Acidalia Planitia, and in Malea Planum. We observe a significant hemispheric asymmetry, with more than three times as many pedestal craters located in the northern hemisphere (Figure 2). There is a dearth of pedestal craters equatorward of ~40°N and S latitude, with the exception of one area west of Tharsis (0°–15°N; 190°–235°E) in the Medusae Fossae Formation [*Schultz and Lutz*, 1988; *Barlow*, 1993; *Watters et al.*, 2007]. All 71 of the pedestal craters with marginal pits are located in Utopia Planitia and Malea Planum, poleward of 48°N and 55°S latitude, respectively (white circles in Figure 1) [*Kadish et al.*, 2008]. The search for pedestal craters with pits was extended to 70°N and S latitude to improve our understanding of their geographic extent.

3.2. Pedestal Crater Attributes

[6] Images of typical pedestal craters are seen in Figure 4, and additional examples are shown with MOLA data (Figure 5); corresponding topographic profiles are in Figure 6. Pedestal crater attributes measured in this study show several significant trends (Figures 7–9 and Tables 2 and 3). Diameters of the crater bowls (Figure 7a) are generally <5 km, with a mean of <2 km; because we did not

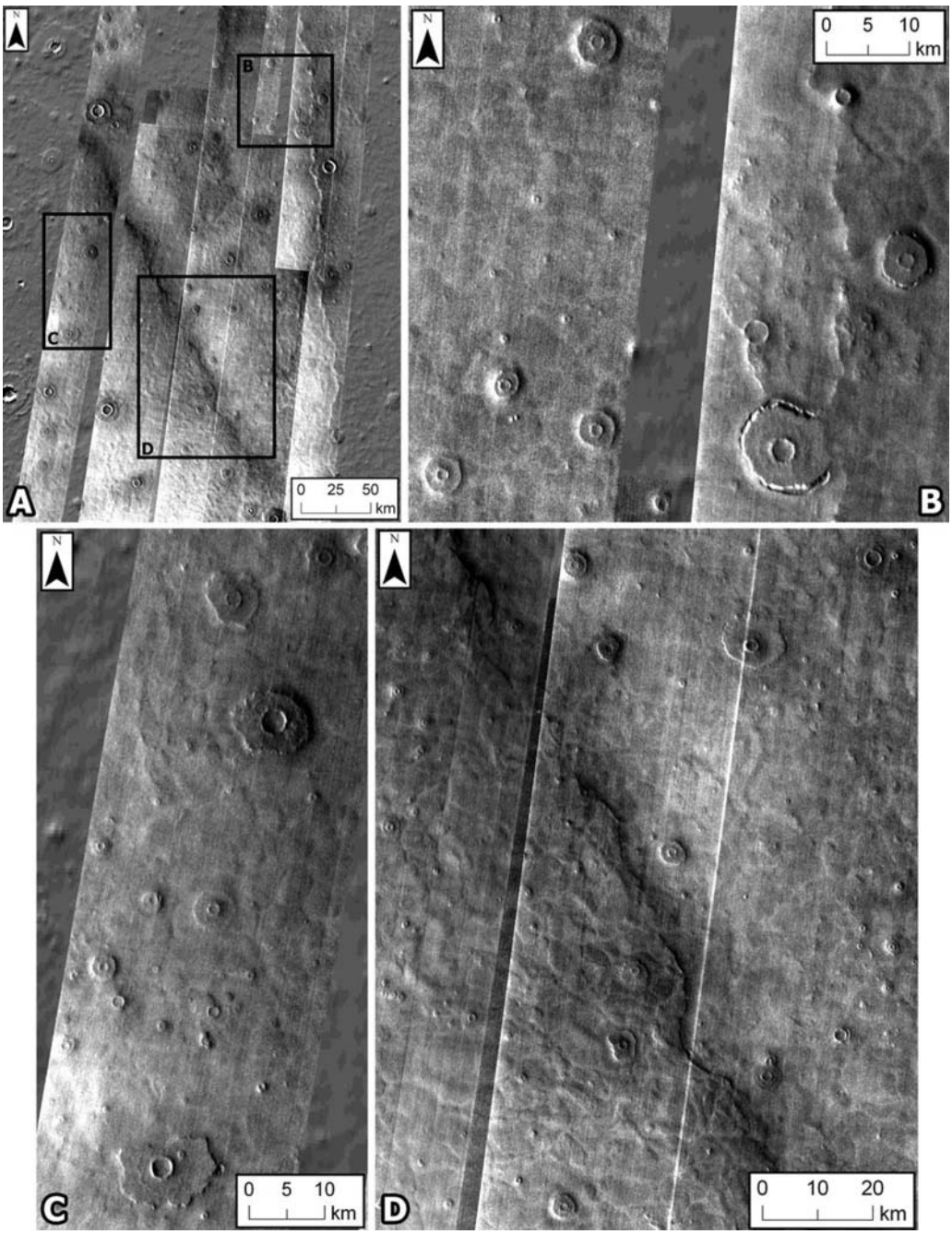

Figure 4. (a) A mosaic of THEMIS IR imagery, with intervening MOLA hillshade data, in Utopia Planitia (101°E, 58°N), displaying a typical pedestal crater field. Black boxes denote the locations of the enlarged regions in Figures 4b–4d. (b) Pedestals with very low Γ values. Marginal pits can be readily identified around two pedestal craters on the right-hand side of the image. (c) Although pedestals are generally circular, this image shows some examples which have sinuous, irregularly shaped perimeters. (d) A larger area showing additional variation in pedestal size and circularity.

measure pedestal craters with diameters <0.7 km, we cannot define an absolute average diameter. Crater bowl diameters tend to increase toward the equator (Figure 8a), and are largest in the Medusae Fossae Formation. This trend is more prevalent in the southern hemisphere, where pedestal craters tend to be larger. The Γ ranges from ∼1 to 2.5 with a mean of 1.1 (Figure 7). Most other types of fresh Martian impact craters have distinctly higher marginal sinuosities [*Barlow*, 2006]; because normal Martian craters lack pedestals, these measurements are based on the perimeters of their ejecta deposits. Extremely high Γ values (>1.4) among pedestal craters are generally found in the Medusae Fossae Formation (see section 4.3 and Figures 13 and 14). Mean Γ values do not appear to be latitude-dependent (Figure 8b).

[7] P/C ratios range from 1.2 to 13; mean values are ∼3.3 at northern middle latitudes and ∼2.5 at southern middle latitudes (Figure 7). Extremely high P/C ratios

Table 1. Pedestal Crater Concentration as a Function of Latitude

Center of 5° Latitude Band (°N)	Number of Pedestal Craters	Number of Pedestal Craters per km^2
−57.5	366	1.08×10^{-4}
−52.5	154	4.00×10^{-5}
−47.5	62	1.45×10^{-5}
−42.5	26	5.58×10^{-6}
−37.5	2	3.99×10^{-7}
−32.5	0	0
−27.5	0	0
−22.5	0	0
−17.5	0	0
−12.5	0	0
−7.5	0	0
−2.5	4	6.33×10^{-7}
2.5	15	2.38×10^{-6}
7.5	30	4.79×10^{-6}
12.5	15	2.43×10^{-6}
17.5	0	0
22.5	0	0
27.5	0	0
32.5	4	7.50×10^{-7}
37.5	38	7.58×10^{-6}
42.5	186	3.99×10^{-5}
47.5	419	9.81×10^{-5}
52.5	630	1.64×10^{-4}
57.5	745	2.19×10^{-4}

(>6) are also usually restricted to the Medusae Fossae Formation (Figures 8c and 13), with the exception of pedestal craters with marginal pits. Pedestal crater P/C ratios are the highest for any Martian crater type [*Barlow*, 2006]. Pedestal crater plateaus are typically elevated ~20–80 m above the surrounding plains on the basis of MOLA measurements (Figures 5 and 6). Preliminary measurements of pedestal heights reveal no correlation with crater or pedestal diameter.

[8] The attributes of pedestal craters with marginal pits (Figures 10 and 11) vary somewhat from those without pits. The morphology of pedestal craters with marginal pits is described in detail by *Kadish et al.* [2008]. To summarize, the outward-facing scarps along the perimeters of some pedestal craters are interrupted by small pits (Figures 10 and 11). Pits often have cuspate shapes and alcove-like features, and tend to be elongated along the pedestal crater scarp. In some cases, pits coalesce to form long moat-like troughs along the pedestal perimeter (Figure 10a). Topographic profiles show that pits, which have typical depths of ~20 m, form on the scarps themselves, not on the surrounding terrain. Furthermore, pit depths do not extend below the elevation the adjacent plains (Figures 10c and 10f). Pit interiors have generally shallow slopes (<10°), and slopes are roughly constant around the perimeter of the pit. We have not observed any significant pole-facing or equator-facing trend for the location of pits around the pedestal scarps. Notable differences between pedestal craters with and without marginal pits are that pedestal craters with pits tend to be larger, with an average crater diameter of 5.1 km and an average P/C ratio of 5.6. In other words, both the crater bowl and the farthest extent of the plateau relative to the crater radius are larger. These pedestal craters with marginal pits have a similar average Γ, 1.06, to those without pits. Pedestal heights of those with pits tend to be about twice as high as those without, having an average height of ~100 m (compare Figures 5 and 10) [*Kadish et al.*, 2008].

[9] As previously mentioned, pedestal craters in the Medusae Fossae Formation are physically distinct from those at middle latitudes and high latitudes (compare Figures 5, 10, and 13). Although the craters themselves, with an average diameter of 2.1 km, are not much larger than pedestal craters without pits at middle latitudes to high latitudes, their pedestals extend much farther; the average P/C ratio of pedestal craters in the Medusae Fossae Formation is 5.4 (Figure 8c). The most distinctive quality of pedestal craters in the Medusae Fossae Formation, however, is a jagged pedestal perimeter (Figures 13 and 14), yielding a mean Γ of 1.64 (Figure 8b). Furthermore, their pedestals are, on average, the tallest of any measured, with mean plateau heights of ~200 m (Figure 13), four times the average height of normal middle-latitude to high-latitude pedestal craters.

4. Discussion

4.1. Trends in Pedestal Crater Attributes

[10] The measurements made in this study reveal a number of significant trends regarding the physical attributes of middle-latitude pedestal craters, as well as those within the Medusae Fossae Formation (Figures 7–9). First, pedestal craters tend to have small crater bowl diameters. Greater than 95% of the pedestal craters we observed have diameters of less than or equal to 2.5 km. Second, pedestal perimeters are extremely circular. More than 69% of pedestal craters measured had Γ values of less than or equal to 1.1, and more than 98% had Γ values less than 1.4. As previously mentioned, the outliers from this measurement are restricted almost entirely to the Medusae Fossae Formation. These low Γ values confirm the general circularity of individual pedestals. Third, more than 97% of pedestal craters have P/C ratios greater than 1.5, and more than 67% have P/C ratios above 2.5. These high P/C ratios, which exceed the typical value of ~1.7 for middle-latitude, single layer ejecta craters on Mars [*Barlow*, 2006], strengthen support for an armoring mechanism that is not limited to direct effects from the ejecta deposit, as discussed in section 4.6.

[11] Latitude-dependent trends for the pedestal crater measurements can be seen in Figure 8, where it is apparent that crater bowl diameters tend to increase as latitude decreases. This trend (Figure 8a) may not be robust owing to the small number of pedestal craters in the southern hemisphere, and is less pronounced in the northern hemisphere. Pedestal circularity (Figure 8b) is relatively constant as a function of latitude, with the exception of the Medusae Fossae Formation. Pedestal craters in the Medusae Fossae Formation show consistently higher values for all measurements taken. Our proposed formation mechanism predicts that Γ values should not be affected by latitude, as is confirmed by our measurements. The P/C ratio does not show a strong increasing or decreasing trend as a function of latitude (Figure 8c), although there are notably higher P/C ratios in the northern hemisphere than in the southern hemisphere. This would be expected if an atmospheric blast plays an important role in the armoring mechanism [*Wrobel et al.*, 2006]; the thicker atmosphere in the northern hemisphere, where the impacts occur at lower elevations, would be more capable of propagating

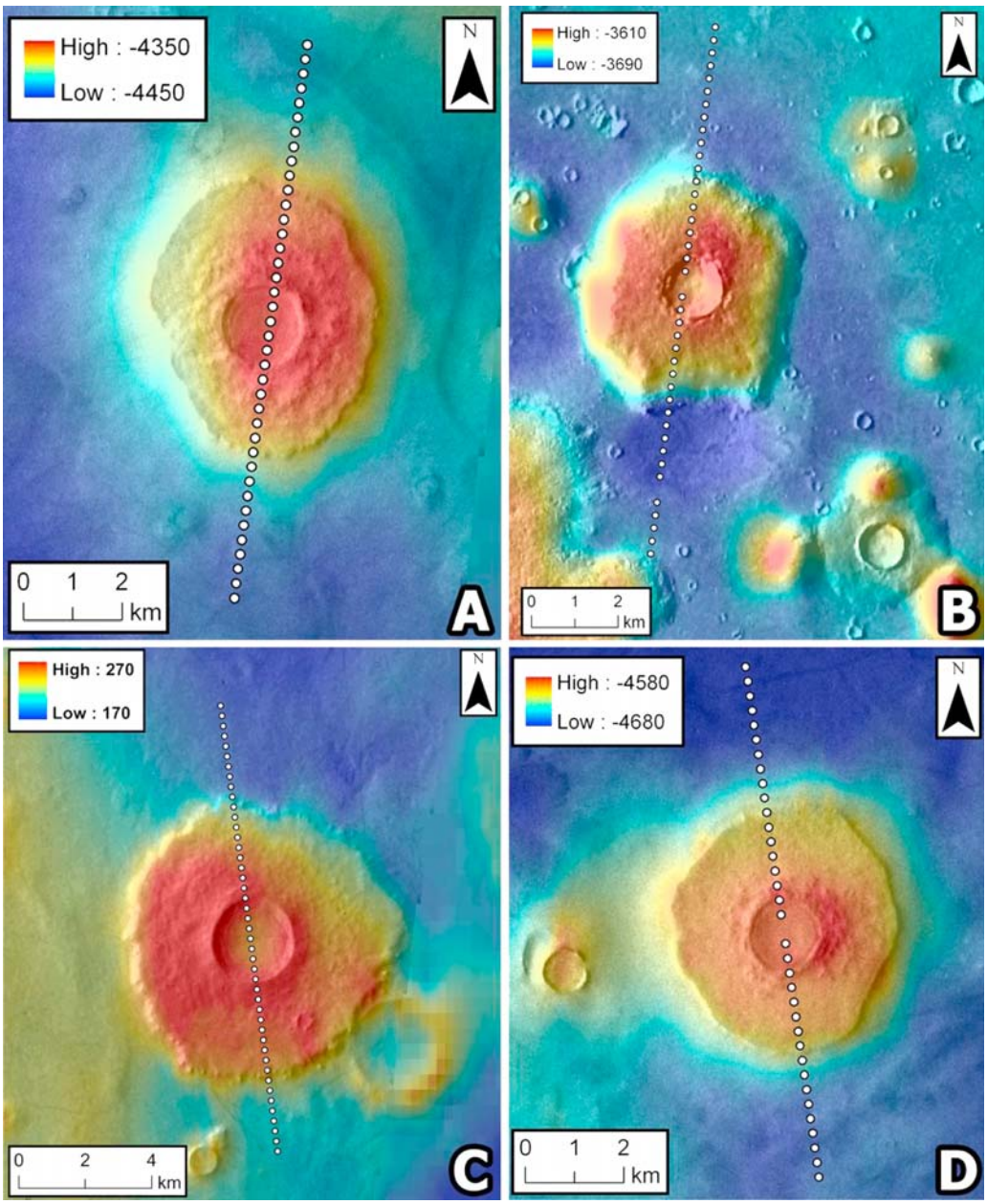

Figure 5. Examples of typical pedestal craters shown in THEMIS VIS data with MOLA altimetry data. Each image has a MOLA track consisting of the shot data, corresponding to a topographic profile seen in Figure 6. These small craters are roughly circular in planform and have crater diameters <2.5 km. The pedestals have relatively smooth, flat tops with well-defined marginal scarps. (a) A subscene of V21963008 (58.6°N, 110.7°E). (b) A subscene of V13575007 (41.6°N, 153.4°E). (c) A subscene of V18359003 (56.9°S, 43.7°E). (d) A subscene of V19230010 (55.8°N, 107.4°E).

the shockwave and thermal pulse, allowing for generally larger pedestals. The data point in the 35 to 40°N bin in Figure 8 includes pedestal craters from 30 to 40°N because so few were present between 30 and 35°N. Even with the lumping of data, these points represent only 24 craters, and thus their deviation from the noted trends is likely due to the statistics of small numbers.

[12] Comparisons of pedestal crater attributes (Figure 9) show a number of interesting results, most notably that the measured characteristics may be largely independent of each other. Pedestal craters tend to have small diameters and low Γ values. However, examination of the extremes for each attribute shows that pedestal craters can have very low Γ values even with large diameters. Conversely, pedestal craters with small diameters can have high Γ values. In addition, pedestal craters in the Medusae Fossae Formation can have both high Γ values and large diameters. Comparing P/C ratio to crater diameter, a similar trend is observed. Pedestal craters usually have low P/C ratios and diameters, but in some instances have large diameters with low P/C ratios, and high P/C ratios with small diameters. Some examples also have large diameters and high P/C ratios. In

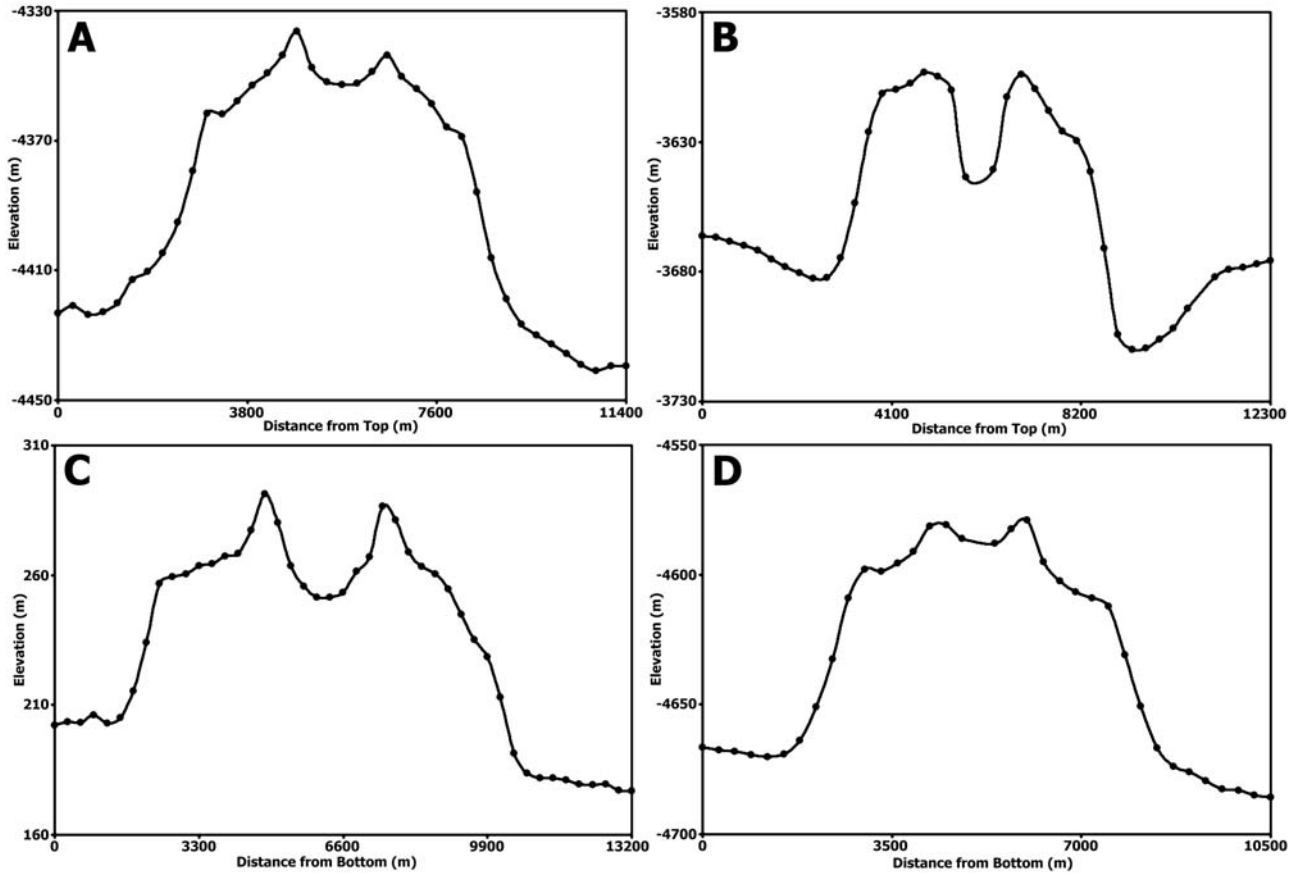

Figure 6. The topographic profiles for the pedestal craters shown in Figure 5, with visible data points corresponding to the MOLA shot data. Vertical exaggerations for each of the profiles are (a) 65X, (b) 55X, (c) 50X, and (d) 47X. Pedestal heights vary from ~50 to 75 m. Pedestal surfaces are extremely flat, with slopes generally <1°, and pedestal scarps have slopes of <5°. In all cases, the crater cavity is entirely above the elevation of the surrounding plains. In some cases (Figures 6a and 6d), infilling of the crater bowl or lowering of the pedestal surface causes the crater floor to be above the height of most of the surrounding pedestal as well.

other words, regression analyses on these data show low R^2 values, suggesting that there are no statistically significant trends. When Γ values are compared to P/C ratios, a slightly positive correlation is observed, with higher P/C ratios corresponding to higher Γ values. This may suggest that larger pedestals (not necessarily larger crater diameters) may not be homogeneously armored, especially near the distal edge of the pedestal, or that larger pedestals are more prone to differential erosion, resulting in asymmetrical pedestal degradation.

4.2. Climate Models and Odyssey GRS Experiment Data

[13] The strong latitude-dependent distribution of pedestal craters suggests a correlation between pedestal craters and the history of climate on Mars. Although the various Martian climate models do not agree precisely on certain climatic details (e.g., ice accumulation rates), a broad consensus does exist in many areas. The common conclusion is that, during periods of high obliquity (>35°), increased insolation to the polar regions during the summer removes volatiles from the polar caps and deposits them at lower latitudes either via precipitation or vapor diffusion into the regolith [e.g., *Forget et al.*, 1999; *Jakosky et al.*, 1995; *Richardson and Wilson*, 2002; *Haberle et al.*, 2003; *Mischna et al.*, 2003; *Mellon et al.*, 2004]. The atmospheric humidity increases, and the latitude at which surface ice is stable moves toward the equator. During periods of low obliquity, this latitudinal limit is usually around 60°, but at higher obliquities, the ice stability zone moves to ~30°. Most models predict increased wind strength during the higher obliquity eras as well, raising the atmospheric dust content. This dust is incorporated into the ice, potentially yielding fine-grained, ice-rich deposits between 30° and 60° latitude in both hemispheres [*Head et al.*, 2003; *Jakosky et al.*, 1995; *Laskar et al.*, 2004]. When the obliquity decreases, the atmosphere dries and the middle-latitude ice-rich layer desiccates. The sublimated ice eventually returns to the poles, leaving behind an ice-poor regolith, although the generally short durations of periods of low obliquity combined with the development of sublimation lags are not likely to result in complete removal of the ice from the middle latitudes [*Head et al.*, 2003; *Mellon et al.*, 1997; *Touma and Wisdom*, 1993]. This movement of ice from the polar regions to the middle latitudes and tropics is expected to operate on time scales of 10^5–

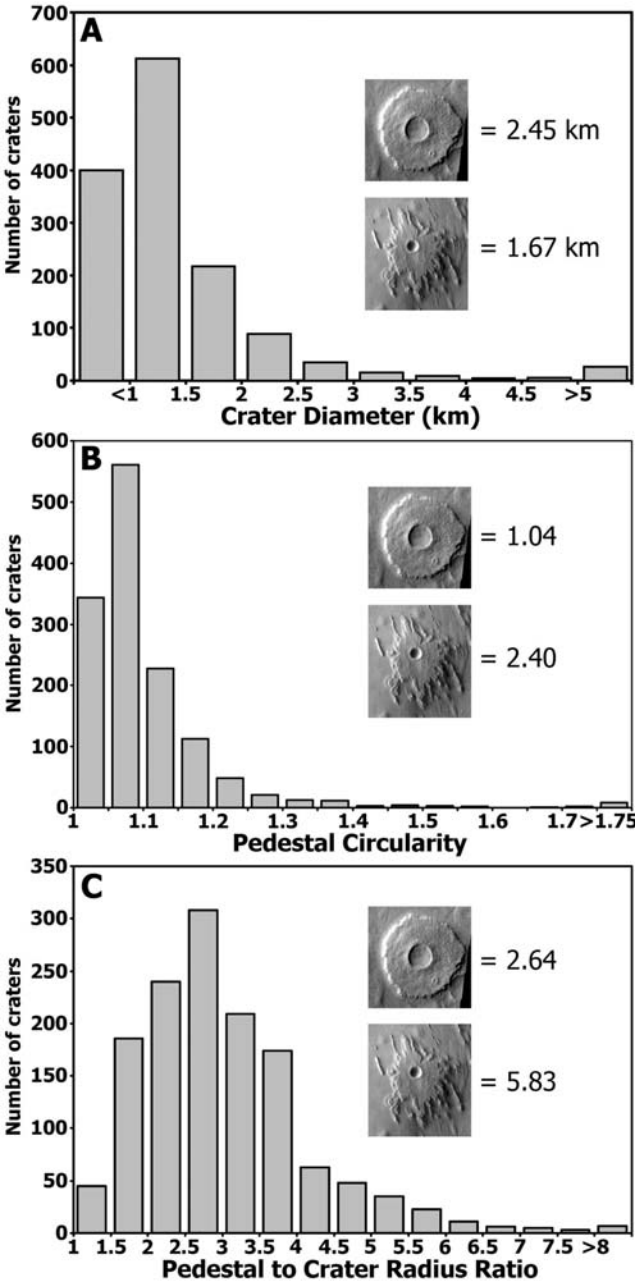

Figure 7. Histograms showing the distribution of three pedestal crater attributes: (a) crater diameter, (b) pedestal circularity (Γ), and (c) pedestal to crater radius (P/C) ratio. For crater diameters, the mode is 1.10 km, with a mean of 1.37 km and a standard deviation of 0.57 km. For Γ values, the mode is 1.04, with a mean of 1.10 and a standard deviation of 0.11. For P/C ratios, the mode is 2.00, with a mean of 3.09 and a standard deviation of 1.22. For each attribute, the values are shown for two pedestal craters, selected to show variation in pedestal morphology. The top crater is in the southern hemisphere and the bottom is in the Medusae Fossae Formation.

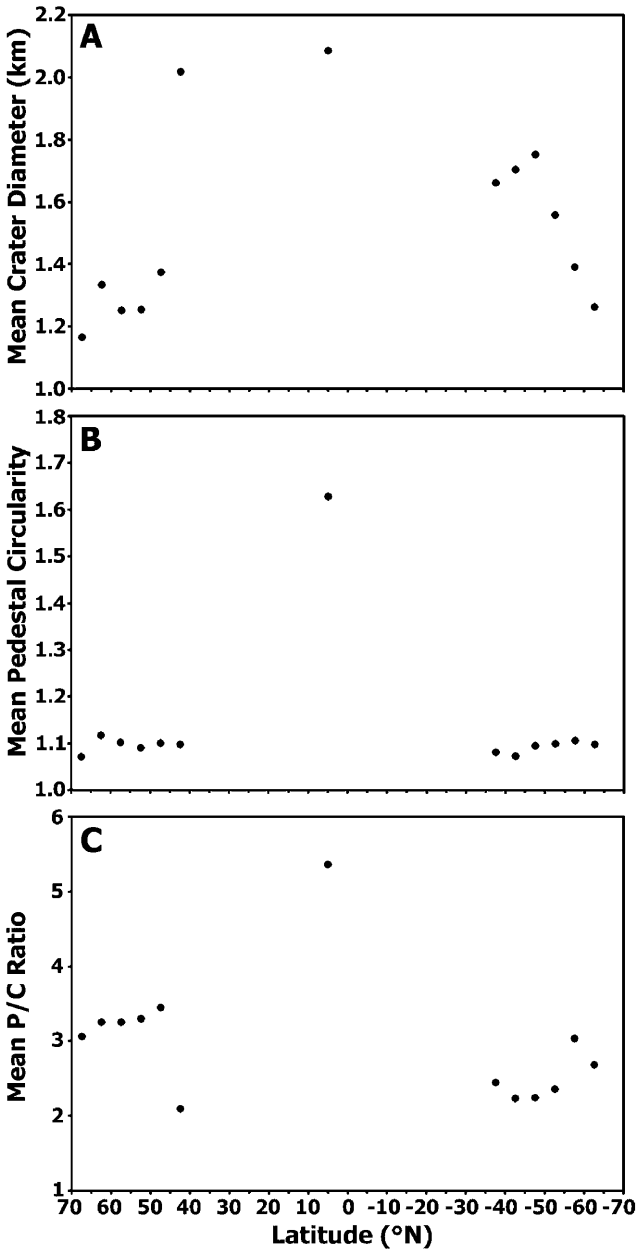

Figure 8. Graphs showing the latitudinal trends in pedestal crater attributes. Data points represent 5° latitudinal bins. The equatorial data point in each graph represents the Medusae Fossae Formation pedestal crater population. (a) Crater diameters appear to increase as latitude decreases. This trend is weaker in the northern hemisphere, where the majority of pedestal craters exist. (b) Γ values for middle-latitude pedestal craters are independent of latitude. (c) P/C ratios are consistently higher in the northern hemisphere than in the southern hemisphere, but show no significant trend as a function of latitude. It is important to note that standard deviations are significant for all data points in these graphs, and as such, trends derived from latitudinal changes of the mean values may not be statistically significant. The mean values and standard deviations for these graphs are shown in Table 3.

10^6 years, and current near-surface ice (upper meter of regolith) near the stability boundary (~60° latitude) is expected to have an age of <500 ka [*Haberle et al.*, 1993; *Mellon et al.*, 2004; *Mischna et al.*, 2003].

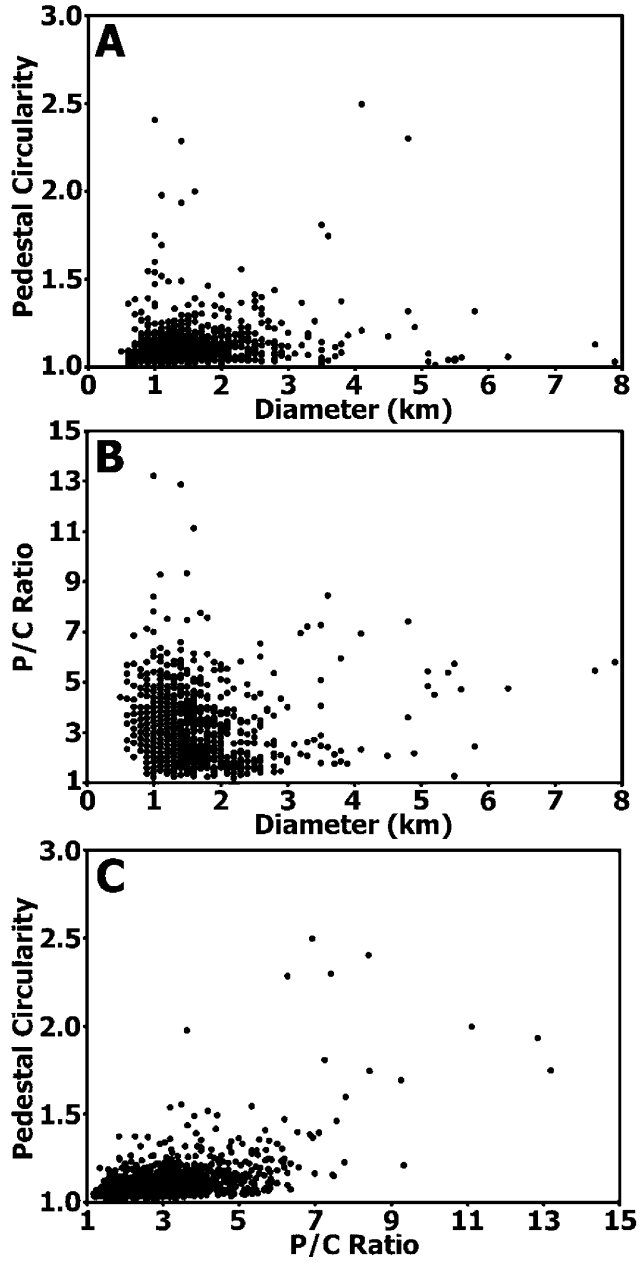

Figure 9. Plots of pedestal crater attributes, exploring possible relationships among crater size, pedestal size, and pedestal circularity: (a) Crater diameter versus Γ (R^2 = 0.039), (b) diameter versus P/C ratio (R^2 = 0.001), and (c) Γ versus P/C ratio (R^2 = 0.286). Most pedestal craters plot in the bottom left of each graph. There is no identifiable correlation between crater diameter and Γ or P/C ratio. There may be a small positive correlation between Γ value and P/C ratio.

[14] The global epithermal neutron data acquired by Mars Odyssey's gamma ray and neutron spectrometer (GRS) provide important information about the current distribution of water ice on Mars [*Boynton et al.*, 2002; *Feldman et al.*, 2002; *Mitrofanov et al.*, 2002], and can thus be used to enhance our understanding of the distribution of pedestal craters. The spectrometer detects to a depth of approximately one meter in the Martian soil, thus measuring the volatile content of the uppermost part of the subsurface. Because pedestals are significantly thicker than one meter, the GRS data cannot directly measure the abundance of volatiles throughout the pedestals. In addition, the GRS data represent the hydrogen content at the current low Martian obliquity. The pedestal craters, however, were likely emplaced during past higher obliquity periods, and the lateral extent of the ice-rich material has been receding poleward since this time. The thermal, epithermal, and fast neutron data can be used to derive water-equivalent hydrogen concentrations in the form of water ice or hydrated minerals [*Boynton et al.*, 2002; *Feldman et al.*, 2002; *Mitrofanov et al.*, 2002]. We compare the GRS water-equivalent hydrogen maps with the distribution of pedestal craters (Figure 12). High levels of water-equivalent hydrogen can be indicative of intact, shallowly buried ground ice covered by desiccated soil [*Boynton et al.*, 2002; *Mellon et al.*, 2004].

[15] Figure 12 reveals a strong latitudinal correlation between the pedestal crater distribution and the concentration of water-equivalent hydrogen. Between 0° and 60°N, the latitudes with the highest hydrogen content (>8 wt% water-equivalent hydrogen) are generally poleward of 50°N, but dip as low as 35°N, matching the pedestal crater distribution in Arcadia Planitia (Figure 12). Between 0° and 65°S, the latitudes with the highest hydrogen content are mostly poleward of 60°S, but reach 50°S near Malea Planum. It is possible that some pedestal surfaces, especially those at higher latitudes, have become reenriched in water ice since they formed. We, however, highlight this correlation between high water-equivalent hydrogen and pedestal crater distribution to show that pedestal craters tend to form where water ice is present near the surface. Note that some small populations of pedestal craters are present in relatively lower water-equivalent hydrogen areas. This is expected during the current period of low obliquity, when the intercrater terrain surrounding some middle-latitude pedestal craters has become desiccated near the surface. However, the locations of these regions coincide with areas that were likely covered by ice-rich deposits during past periods of higher obliquity [e.g., *Mustard et al.*, 2001; *Head et al.*, 2003]. Thus, the current distribution of water-equivalent hydrogen is consistent with the interpretation of the pedestal craters resulting from obliquity-

Table 2. Pedestal Crater Attributes[a]

Type of Pedestal Crater	Mean Diameter	Mean Pedestal Height	Mean Pedestal Circularity	Mean Pedestal to Crater Radius Ratio
Nonpitted, middle latitude to high latitude	<2 km	~50 m	1.10	3.09
Equatorial (Medusae Fossae Formation)	2.1 km	~200 m	1.64	5.36
Pedestals with marginal pits	5.1 km	~100 m	1.06	5.62

[a]Because pedestal craters with diameters less than 0.7 km were identified but not included in this study, the mean diameter for middle-latitude pedestal craters without marginal pits is specified as less than 2 km.

Table 3. Mean Pedestal Crater Attributes with Standard Deviations as a Function of Latitude

Center of 5° Latitude Band (°N)	Mean Diameter (km)	Standard Deviation of Diameter	Pedestal Circularity	Standard Deviation of Circularity	Pedestal to Crater Radius Ratio	Standard Deviation of P/C Ratio
−67.5	1.26	0.39	1.10	0.07	2.68	0.77
−62.5	1.39	0.72	1.11	0.06	3.03	1.11
−57.5	1.56	0.67	1.10	0.07	2.35	0.83
−52.5	1.75	0.60	1.09	0.07	2.24	0.74
−47.5	1.70	0.57	1.07	0.03	2.23	0.75
−42.5	1.66	0.46	1.08	0.06	2.44	0.90
0.0	2.08	1.25	1.63	0.43	5.36	3.61
37.5	2.02	0.91	1.10	0.06	2.09	0.93
42.5	1.37	0.47	1.10	0.09	3.44	1.37
47.5	1.25	0.45	1.09	0.09	3.30	1.12
52.5	1.25	0.42	1.10	0.09	3.25	1.24
57.5	1.33	0.61	1.12	0.13	3.25	1.04
62.5	1.16	0.21	1.07	0.03	3.06	1.12

driven climate change, having formed during periods of higher obliquity.

4.3. Pedestal Craters in the Medusae Fossae Formation

[16] The presence of pedestal craters in an equatorial region (Figures 1, 13, and 14), from about 5°S to 15°N, appears inconsistent with a sublimation-driven model of pedestal crater formation; the closest pedestal craters to the Medusae Fossae Formation population are at 33°N. The formation mechanism for the Medusae Fossae Formation pedestal craters may be closely related to the origin of the fine-grained material that composes the Medusae Fossae Formation. Researchers, however, have been unable to reach a consensus on the exact source of its material [e.g., *Barlow*, 1993; *Bradley et al.*, 2002; *Hynek et al.*, 2003]. If the Medusae Fossae Formation resulted from pyroclastic fall or eolian deposits, it may never have contained ice-rich material [*Scott and Tanaka*, 1982; *Hynek et al.*, 2003]. In this case, pedestal crater formation via sublimation of the surrounding terrain would not be possible. If, however, the Medusae Fossae Formation was created from polar layered deposits during polar wander [*Schultz and Lutz*, 1988] or airborne volatile-rich material deposited locally during a period of high obliquity [*Head and Kreslavsky*, 2004] then it may have had the ice-rich material necessary for sublimation-formed pedestal craters.

[17] The polar layered deposit hypothesis postulates that the deposits formed during a period of polar wander prior to the early stages of Tharsis volcanism [*Schultz and Lutz*, 1988]. The primary evidence for an ice-rich origin came from Viking images of exhumed impact basins and small-scale layering. The opposing argument notes that a polar origin is unlikely based on the time scales required for such an extreme change in spin axis orientation [*Bradley et al.*, 2002; *Tanaka*, 2000]. Analyses of observed tectonic features on Mars are also inconsistent with the lithospheric stresses necessary for the magnitude and timing of the proposed polar wandering [*Grimm and Solomon*, 1986]. Digital elevation models from MOLA data showed that the Medusae Fossae Formation had strikingly similar topography to polar layered terrain [*Head*, 2000], leading to the interpretation that emplacement took place during periods of higher obliquity [*Head and Kreslavsky*, 2004]. The hypothesis that the Medusae Fossae Formation contained ice-rich material deposited during high obliquity is based on climate model predictions [*Richardson and Wilson*, 2002; *Haberle et al.*, 2003; *Mischna et al.*, 2003], gamma ray spectroscopy (GRS) data showing elevated hydrogen in the region [*Boynton et al.*, 2002; *Feldman et al.*, 2002], and calculations of the obliquity history of Mars [*Laskar et al.*, 2004]. This is further supported by geomorphological, stratigraphic, and surface roughness evidence, which suggest the emplacement of an unusually smooth, ice-rich unit interrupted by periods of erosion and volatile loss [*Head and Kreslavsky*, 2004].

[18] From the preceding arguments, it is certainly plausible that the Medusae Fossae Formation contained ice-rich material at some point in its past. Recently, *Watters et al.* [2007] used Mars Advanced Radar for Subsurface and Ionosphere Sounding (MARSIS) data to calculate a real dielectric constant and estimate dielectric losses for the Medusae Fossae Formation. The results were consistent with either a substantial water ice component or an anomalously low-density, ice-poor material [*Watters et al.*, 2007]. From this, we cannot rule out the possibility of a dry pyroclastic fall origin. The distinct geomorphology of pedestal craters in the Medusae Fossae Formation (Figures 13 and 14) suggests that they may have formed through a different process than those in the middle latitudes to high latitudes. Not only are the Medusae Fossae Formation pedestal craters more sinuous/jagged and have farther extending plateaus, but they also excavate to much greater depths; Medusae Fossae Formation pedestal crater bowls can extend hundreds of meters below the elevation of the surrounding terrain, whereas the basins of middle-latitude to high-latitude pedestal craters are most often entirely above the elevation of the adjacent plains (compare profiles in Figures 6 and 13). The shallow depths of middle-latitude and high-latitude pedestal crater bowls may be due, in part, to infilling, which likely results from accumulation of material within the crater bowl either from local eolian dust deposits or from subsequent large-scale, ice-rich dust deposits caused by obliquity changes. The extreme excavation depths in the Medusae Fossae Formation apply to all craters, not just pedestal craters; craters in the Medusae Fossae Formation generally have increased depth/diameter ratios. Simple craters are roughly 79% deeper in the Medusae

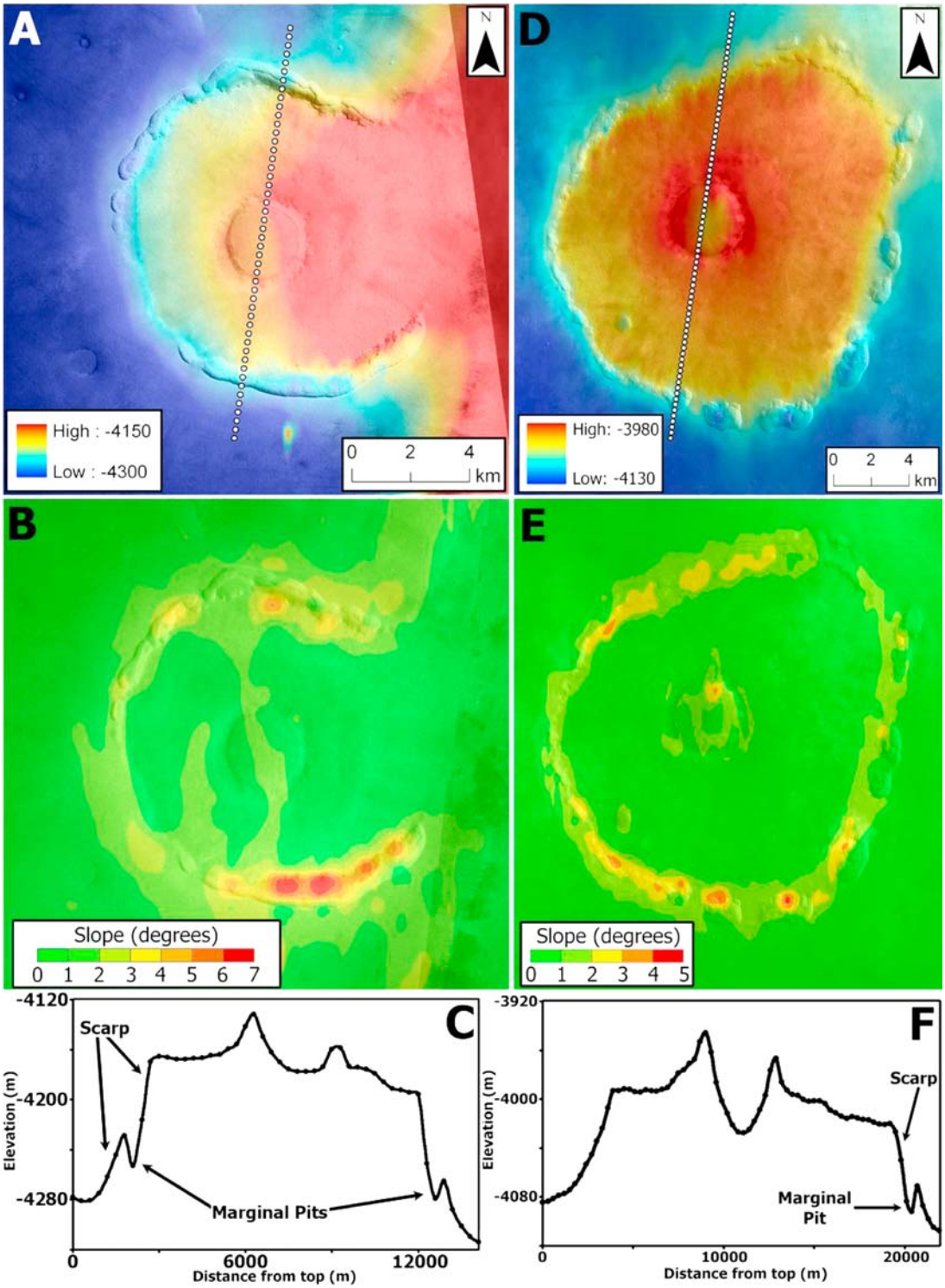

Figure 10. Two examples of pedestal craters with marginal pits, shown in (a, d, e) CTX data and (b) THEMIS VIS data, all with MOLA altimetry data. Corresponding slope maps, derived from the MOLA data, are shown in parts Figures 10b and 10e. (c and f) Profiles of the craters using MOLA shot data are shown, with corresponding data points on the images in Figures 10a and 10d, respectively. The vertical exaggerations are 44X (Figure 10c) and 67X (Figure 10f). Both the slope maps and profiles reveal that the tops of the pedestals are remarkably flat: as flat as the smooth surrounding terrain. The pits marking the pedestal margins generally have slopes of less than 7°, although these slopes are difficult to measure given the small size of the pits and the 300 m spacing between MOLA data points.

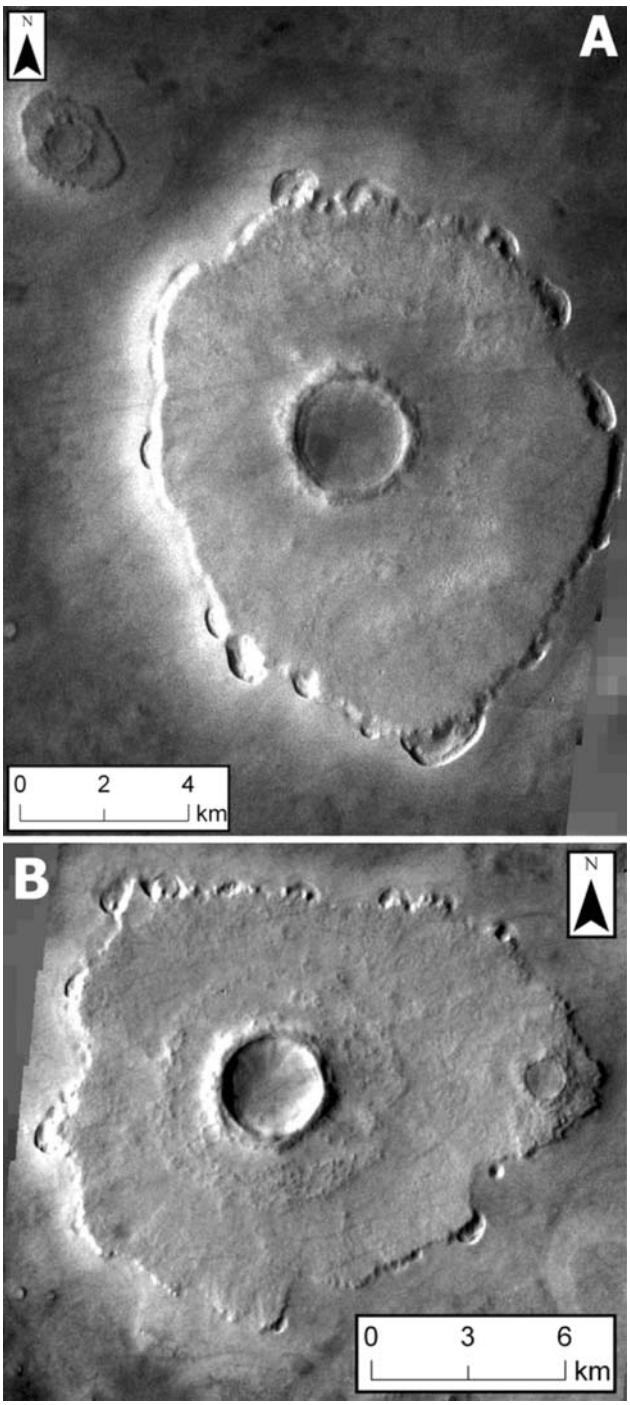

Figure 11. Additional examples of pedestal craters with marginal pits shown in THEMIS VIS data. (a) A subscene of V05726010 (58.5°N, 113.7°E). Pits have formed around most of the pedestal margin, some of which contain isolated mesas. (b) A subscene of V13714004 (56.9°N, 106.9°E). The surface of this pedestal crater is contiguous with the surface of a smaller pedestal crater to the east. The ejecta deposit of the larger pedestal crater is completely superposed on the pedestal surface. Pits are primarily located on the northern and western portions of the pedestal margin. Although both examples have high P/C ratios, the extent of the ejecta deposit can be clearly distinguished in this case, making it readily apparent that the armored surface of the pedestal extends more than twice the distance of the ejecta deposit.

Fossae Formation than craters with the same diameters in other areas [*Barlow*, 1993]. These high depth/diameter ratios have been attributed to its fine-grained, easily erodible and compactable material [*Barlow*, 1993]; laboratory experiments confirm that impacts into fine-grained material can have dramatic effects on the resulting impact morphology [*Schultz*, 1992]. The high P/C ratios of Medusae Fossae Formation pedestal craters may be related to the extreme excavation depths; more material is removed from the crater bowls, which corresponds to greater volumes of material in the pedestals. Alternatively, the high P/C ratios may suggest that the armoring mechanism is more efficient in this fine-grained region. The presence of yardangs and surface textures indicative of eolian erosion adjacent to and contiguous with pedestal craters in the Medusae Fossae Formation suggest that eolian deflation likely played an important role in their formation (Figures 13b and 14c). The Medusae Fossae Formation is also devoid of pedestal craters with marginal pits. If marginal pits do result from sublimation processes in accordance with our model, this complete absence of pits suggests that ice-rich material is not present in the Medusae Fossae Formation pedestals. From this, we conclude that, although it is possible that pedestal craters in the Medusae Fossae Formation formed via the same mechanism as middle-latitude and high-latitude pedestal craters, owing their distinct morphologies to the unique target material of the Medusae Fossae Formation, it is plausible that these features form through a different process based primarily on eolian deflation.

4.4. Ages

[19] Determining the age of a pedestal crater population cannot be done using conventional crater counting techniques [e.g., *Hartmann*, 1966; *Hartmann and Neukum*, 2001; *Hartmann*, 2005] that date the surfaces on which the craters are emplaced because the surrounding surface has been repeatedly removed and redeposited. Despite this limitation, we can place some constraints on the timing of the formation of the pedestal crater population using a combination of methods and observations (Figures 15 and 16). From our survey, we have observed that pedestal craters are generally morphologically fresh (Figures 4 and 5). Crater rims are usually well preserved (Figure 6), and pedestal surfaces are rarely degraded at THEMIS VIS resolution (18 m/pix).

[20] The geographic distribution of pedestal craters shows that a significant portion of the population is located on Amazonian-aged units in the northern lowlands [*Tanaka et al.*, 2003] and in the north polar region [*Tanaka*, 2005]. This superposition of pedestal craters on young surfaces supports the notion that pedestal craters formed recently. In particular, pedestal craters are concentrated on the Vastitas Borealis Formation (AHvh), as well as smooth (Als_1) and coarse (Alc) lobate materials, which are late Hesperian to early-to-mid Amazonian in age [*Tanaka et al.*, 2003]. Additionally, *Tanaka et al.* [2003] map a smaller population of pedestal craters at high latitudes, which they note is present on Amazonian materials such as polar layered deposits (Apl_1), as well as Hesperian plains including the Scandia unit (Hs).

[21] If marginal pits form via sublimation, then these features may also support a young age. These pits appear morphologically fresh, with pristine rims and no signs of infilling. Although the sublimation of volatiles is inhibited

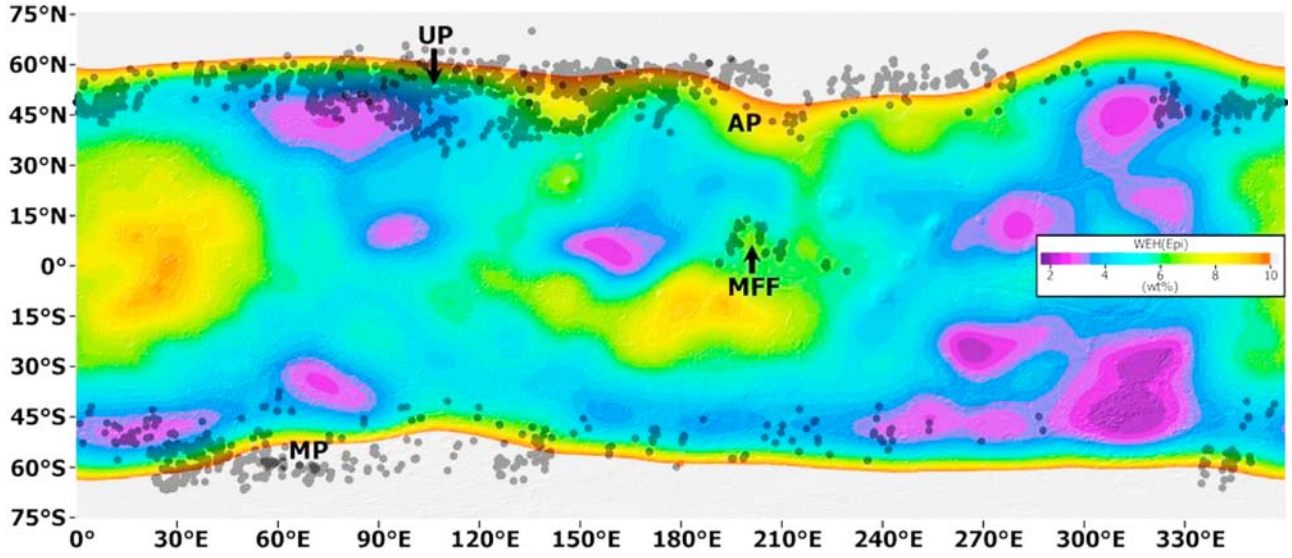

Figure 12. The pedestal crater distribution (black dots) shown on the water-equivalent hydrogen map, derived from the GRS epithermal neutron data [*Feldman et al.*, 2002]. Pedestal craters are primarily located in green, yellow, red, and gray regions, corresponding to greater than 6 wt% water-equivalent hydrogen in the current environment. The general correlation supports the interpretation that pedestal craters form in regions that are likely to contain ice-rich material at higher obliquities [e.g., *Head et al.*, 2003]. Regions of interest are labeled on the map: Utopia Planitia (UP), Arcadia Planitia (AP), the Medusae Fossae Formation (MFF), and Malea Planum (MP). Meridional profiles and zonal averages showing water-equivalent hydrogen as a function of latitude have been previously published [*Feldman et al.*, 2004a, 2004b, 2005], and the raw neutron fluxes as a function of latitude are also available [*Boynton et al.*, 2002].

by the armored pedestal surface, it is not completely prevented. Diffusive exchange of water between ground ice and the atmosphere at middle latitudes is largely affected by obliquity oscillations, and will result in periodic saturation and desiccation of the upper few meters of soil [*Mellon and Jakosky*, 1995]. During periods of low obliquity, higher soil temperatures and lower atmospheric water content at middle latitudes makes ground ice unstable [*Mellon and Jakosky*, 1993, 1995; *Mellon et al.*, 2004]. Currently, pedestal craters with marginal pits are concentrated around 60° latitude in both hemispheres, which is the latitudinal boundary for stable water ice, as shown by GRS data: the terrain is hydrogen-rich poleward of 60° latitude [*Feldman et al.*, 2002]. If the indurated pedestal surface drastically restricts the diffusive exchange process, pedestal craters may maintain ground ice within the upper few meters of their pedestals. However, the armoring may be weaker near the pedestal margins, as discussed in section 4.8, allowing for more rapid diffusive exchange of volatiles between the pedestal and the atmosphere. As mentioned in section 4.2, *Mellon et al.* [2004] argue that ice in the dynamic saturation/desiccation zone should be relatively young (<500 ka). It is thus possible that on the basis of our observations, marginal pits represent an active sublimation process and are still developing, forming connected pits and moat-like structures around pedestal craters. In this case, near-surface ice in the pedestals must be young, and thus the pedestals themselves must be young. We recognize, however, that this evidence is model-dependent, and we cannot, at this time, be certain of the ages of these pits.

[22] Although crater counting cannot provide an absolute age for the pedestal crater population, it can provide a lower limit for how long the population took to form. We used a polygon that delineated the current geographic location of pedestal craters within our survey area to calculate the area on which pedestal craters are capable of forming. This polygon was designed to follow the borders established by the outer geographic reaches of the pedestal crater populations so as to avoid an overestimation of the counting area. Using this area with the measured diameters of 1363 pedestal craters (1027 from the northern hemisphere and 336 from the southern hemisphere), we find a best fit of approximately 50 Ma (Figure 15) based on isochrons from *Hartmann* [2005]. When considering the northern and southern hemisphere populations separately, taking into account distinct crater counting areas, the best fits derived from the *Hartmann* [2005] isochrons are approximately 65 Ma and 32 Ma, respectively. This population of 1363 pedestal craters, which is ~50% of the total mapped, was identified using THEMIS IR image releases 1 through 13 (orbit range 816 to 13499), which has >88% coverage between 60°N and 60°S. Measurements of the diameters of the additional 1333 pedestal craters identified while surveying THEMIS IR image releases 14–23 are currently being acquired. The set of images from THEMIS IR image releases 14–23 increases the coverage between 60°N and 60°S to >96%, and improves the quality of images in many areas. Because we used half of the measured pedestal crater population for the size frequency distribution (Figure 15), our best fit is necessarily an underestimate. However, for young surfaces (<3 Ga), we

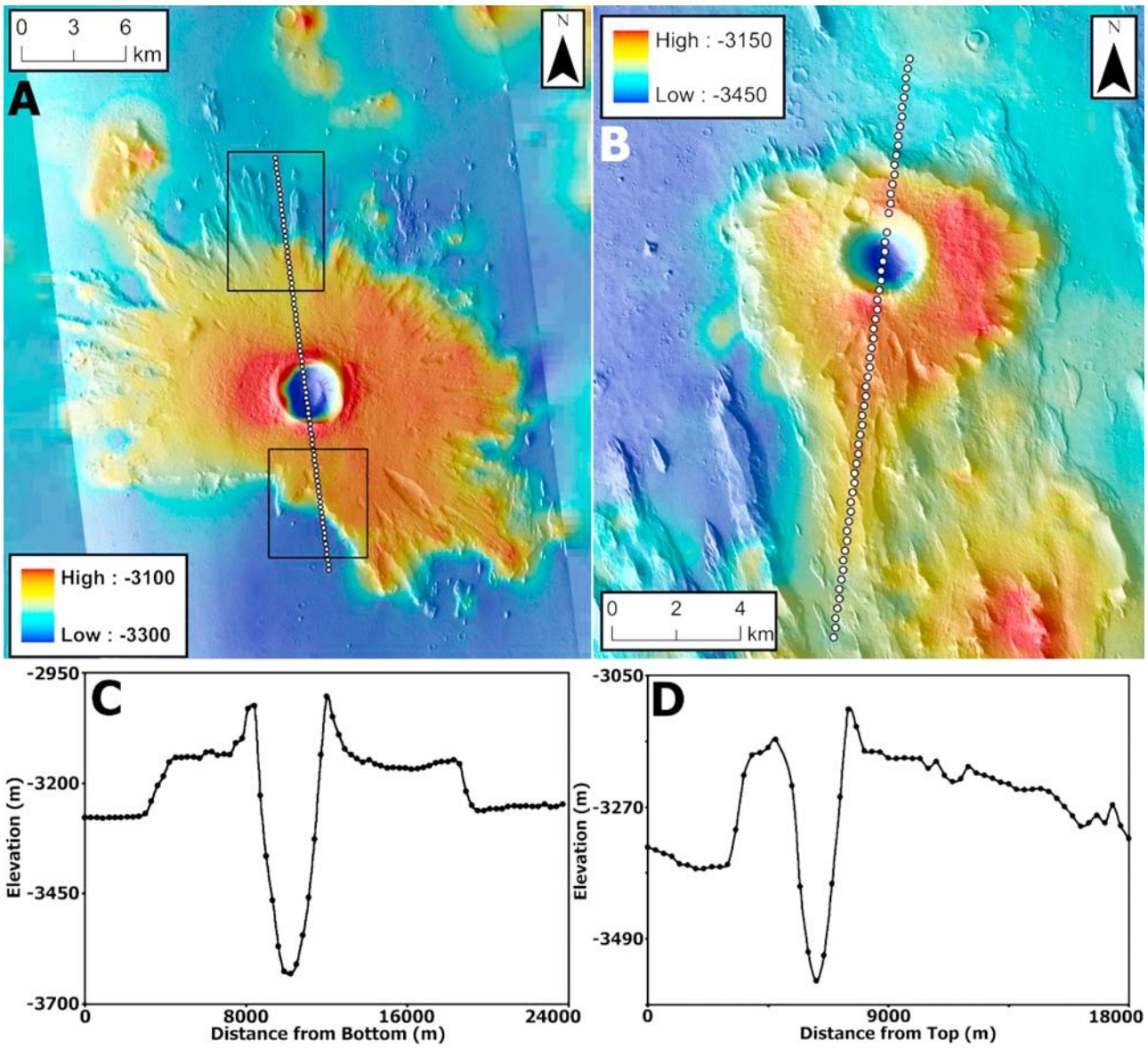

Figure 13. Pedestal craters in the Medusae Fossae Formation, shown in CTX data with MOLA altimetry data, each with a corresponding MOLA profile. These pedestal craters are morphologically distinct from typical pedestal craters at middle latitudes and high latitudes, as shown in Figures 4 and 5. (a) A subscene of P06_003253_1875_XI_07N163W (7.7°N, 196.2°E). Note the jagged pedestal perimeter, exemplifying the high Γ values of pedestal craters in the Medusae Fossae Formation. Black boxes in this image denote the locations of enlarged images in Figure 14. (b) A subscene of P06_003556_1895_XI_09N156W (9.3°N, 203.8°E). The pedestal crater is surrounded by a field of yardangs, some of which are contiguous with the pedestal surface. These pedestal craters have high Γ values (2.5 and 1.7 for Figures 13a and 13b, respectively). The crater in Figure 13a has a high P/C ratio (6.9), while that of the crater in Figure 13b is low (2.6). (c and d) The profiles of the pedestal craters show the anomalously deep crater bowls observed throughout the Medusae Fossae Formation, reaching depths hundreds of meters below the surrounding plains. Despite the large pedestal heights (∼150–200 m), no marginal pits are present and none have been observed on any pedestal margins in the Medusae Fossae Formation.

can assume a relatively constant crater flux [e.g., *Neukum et al.*, 2001]. Thus, doubling the number of pedestal craters on the surface will double the derived best fit time from 50 Ma to 100 Ma, assuming that the frequency distribution of pedestal crater diameters does not vary significantly between the 1363 used and the 1333 being measured.

[23] This derived time implies that the pedestal crater population could have formed in a minimum of ∼100 Ma, assuming the continuous presence of the proposed latitude-dependent, ice-rich deposit. However, the time required to form the observed population is necessarily greater than 100 Ma because the deposit is not currently present and a

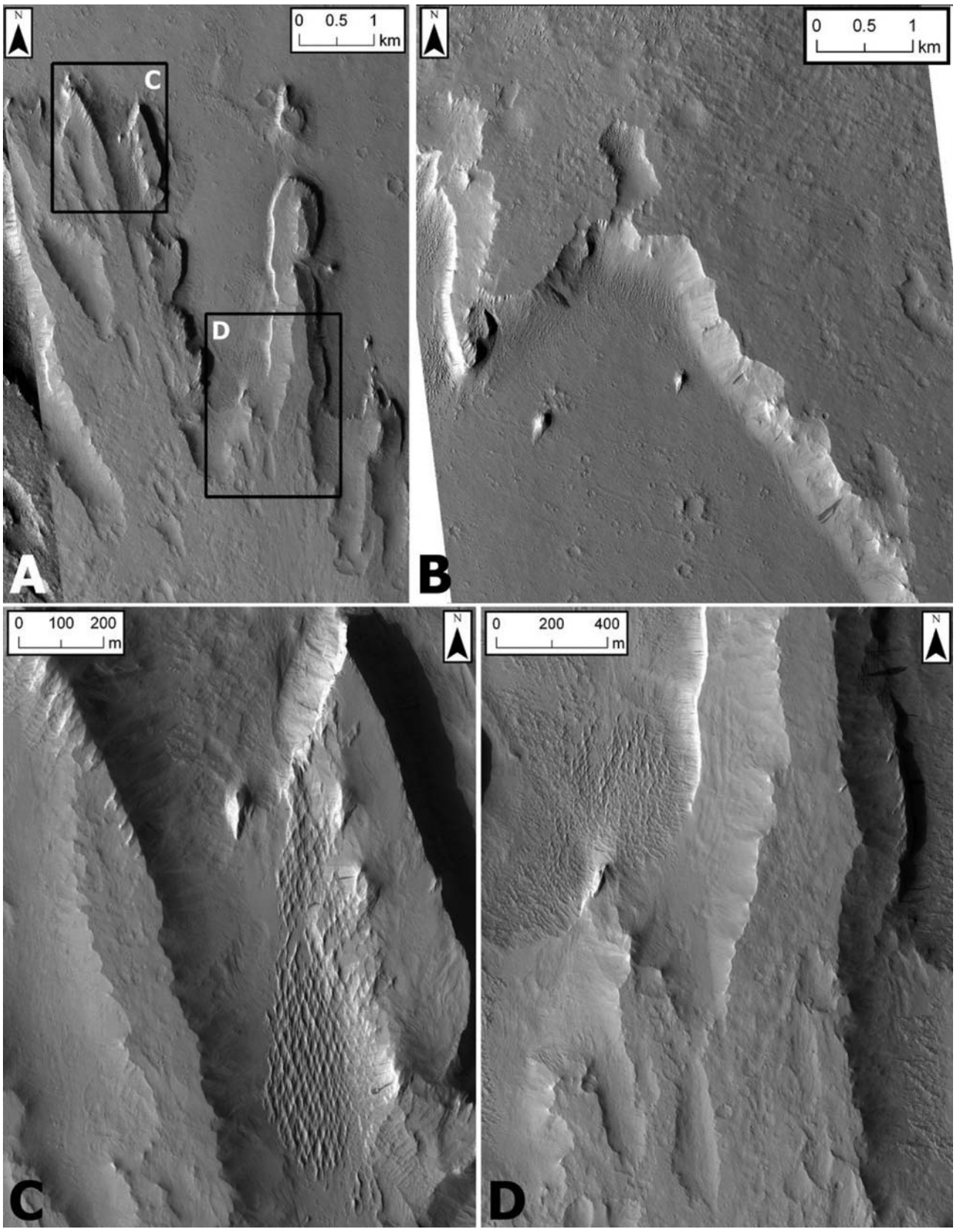

Figure 14. (a) Enlarged regions from Figure 13, showing the detailed morphology of pedestals in the Medusae Fossae Formation. The locations of Figures 14c and 14d are outlined. (b) A section of the south facing pedestal scarp. Small yardangs are present in the surrounding terrain. (c) Erosion of the pedestal is readily apparent at this scale, with dunes present where the pedestal is being eroded. (d) The pedestal scarp appears to have two distinct tiers here, with dunes at the base of the scarp.

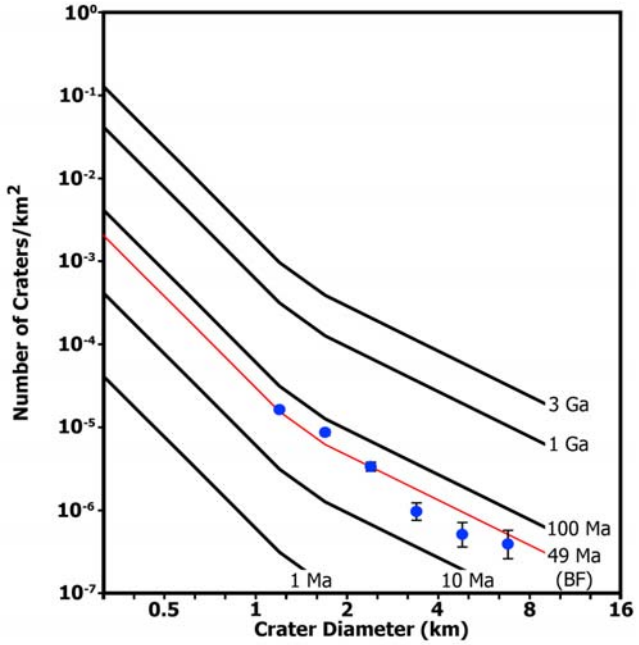

Figure 15. A size frequency distribution using isochrons from *Hartmann* [2005] for 1363 pedestal craters in THEMIS IR data releases 1 through 13. Error bars were calculated using the 90% confidence interval from an inverse gamma function. Although a typical size-frequency distribution is not appropriate for estimating the age of the pedestal crater population, the data do provide a lower limit for the amount of time necessary to form the observed pedestal crater population. Because we used half of the total number of pedestal craters identified in this study for the size frequency distribution, the best fit (BF) of approximately 50 Ma should be doubled to 100 Ma. The best fit line was determined by assigning an isochron to the data and minimizing the misfit. The result suggests that it would have taken at least ~100 Ma at higher obliquity (with the ice-rich substrate emplaced at middle latitudes) to form the measured pedestal crater population. On the basis of the modeled obliquity variations by *Laskar et al.* [2004], and the state of preservation of these features, it is likely that this amount of time at high obliquity occurred in the Amazonian period.

robust solution for the last 20 Ma of Martian obliquity history [*Laskar et al.*, 2004] shows periods of low obliquity for the last 3–5 Ma, and potentially widely variable obliquity for the last 250 Ma. Additional work on dating pedestal craters will be possible when more high-resolution imagery is available of pedestal surfaces. These images can then be used to perform crater counts on the pedestal surfaces themselves, effectively dating the age of the surface of the ice-rich deposit, and thus of the regional pedestal crater population.

[24] Global climate modeling at a range of obliquities (from 15° to 45°) to investigate the recent formation and evolution of the north polar layered deposits [*Levrard et al.*, 2007] and modeling of the fate of polar water at 45° obliquity [*Forget et al.*, 2006] strongly suggest that polar ice migrates rapidly to the tropics (equatorward of 25° latitude); all the simulations displayed a direct exchange between the northern polar cap and high topography equatorial regions [*Forget et al.*, 2006; *Levrard et al.*, 2004, 2007]. Only with obliquities lower than today (~15° and 20°) and an equatorial source were large-scale accumulations of ice observed poleward of 60° latitude in both hemispheres, with some excursions into the middle-latitude regions [*Levrard et al.*, 2004]. Other models [*Mischna et al.*, 2003; *Mischna and Richardson*, 2005], however, show significant deposition of ice at increasingly lower latitudes as obliquity increases. In these models, the polar reservoir is eventually exhausted and equatorial ice dominates.

[25] On the basis of the modeled Martian obliquity history over the past 20 Ma, and possible histories over the past 250 Ma [*Laskar et al.*, 2004], it is likely that pedestal craters formed during multiple high obliquity events, on successive deposits of ice-rich material at middle latitudes and high latitudes. This interpretation is supported by numerous instances of pedestal craters being completely superimposed or partially draped over other pedestal craters (Figure 16). Because these excursions to higher obliquity have likely been common throughout the Amazonian [*Laskar et al.*, 2004], it is plausible that an ice-rich substrate has been emplaced at middle latitudes for much greater than the 100 Ma lower limit, and thus that pedestal craters are more broadly distributed in age throughout the Amazonian.

4.5. Hemispheric Asymmetry in Pedestal Crater Distribution

[26] There is a notable hemispheric asymmetry in the distribution of pedestal craters, with more than three times as many in the northern hemisphere as in the southern hemisphere between 60°N and 65°S latitude. There are two probable factors influencing the observed preferential formation in the northern hemisphere. These include (1) differences in atmospheric thickness, and thus in the overlying atmospheric water column abundance, defined as the amount of water vapor in the atmosphere above a defined surface area, and (2) the availability/distribution of fine-grained material and variations in surface roughness.

[27] The northern lowlands are, on average, about 6 km lower in elevation than the southern highlands. As such, the low elevation of the northern hemisphere plains is overlain by a thicker atmospheric layer, generally supporting a greater atmospheric water column abundance; this has been empirically confirmed by a number of instruments including: Mars Atmospheric Water Detector (MAWD) on Viking [*Farmer et al.*, 1977], Thermal Emission Spectrometer (TES) on Mars Global Surveyor [*Smith*, 2002, 2004; *Sprague et al.*, 2006], and Spectroscopy for Investigation of Characteristics of the Atmosphere of Mars (SPICAM) on Mars Express [*Fedorova et al.*, 2006]. Volatiles from the polar regions are suspended in the Martian atmosphere and transported to the middle latitudes during periods of high obliquity. Following atmospheric transport, the volatiles are precipitated as ice and snow on the surface, or diffuse into the regolith [e.g., *Jakosky*, 1983; *Fanale et al.*, 1986; *Mellon et al.*, 2004]. It is possible that, during periods of high obliquity, the thinner atmosphere in the southern highlands is limited in its capacity to transport volatiles to middle latitudes; although the transport process may be equally efficient in each hemisphere, the greater thickness of the atmosphere overlying the northern hemisphere simply allows for a greater quantity of water vapor to be transported. In the southern hemisphere, this could yield a

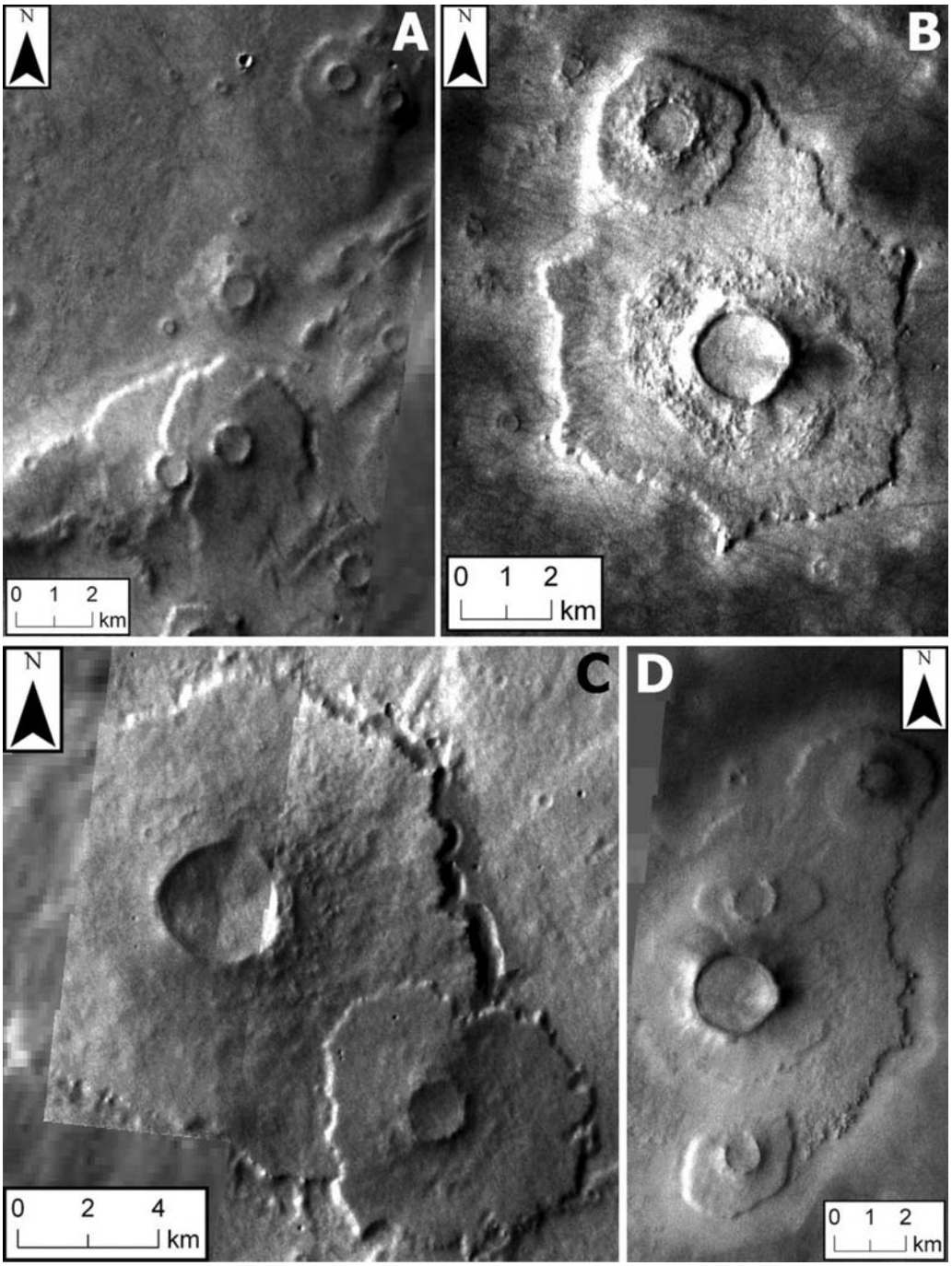

Figure 16. Examples of draped and overlapping pedestal craters shown in THEMIS VIS data. These superposition relationships suggest the formation of pedestal craters from multiple episodes of deposition of an ice-rich substrate, possibly from separate high obliquity periods. (a) A subscene of V09959003. Near the bottom of the image, one pedestal crater is draped over another. The margin of the overlying pedestal curves around the crater rim of the underlying pedestal. Another example of overlapping pedestal craters is visible in the top right of the image. (b) A subscene of V21415004 (57.1°N, 78.5°E). This example shows the limited extent of the rough-textured ejecta deposit superposed on the smooth pedestal surface; the pedestal surface has a greater radial extent than the ejecta deposit in all directions. A small marginal pit exists on its eastern scarp. (c) A mosaic from V18046009 and V18358008 (61.0°S, 71.0°E). The larger crater has marginal pits along its eastern perimeter. The smaller crater is draped over this scarp, truncating one of the pits. (d) A subscene of V20142002 (59.0°N, 80.4°E). Multiple overlapping pedestal craters are visible in this image. Similar to the example in Figure 16b, the outline of the ejecta deposit of the largest crater in the scene can be identified and is completely superposed on the pedestal surface.

thinner ice-rich deposit, which may not extend as close to the equator as in the northern hemisphere. This effect would tend to make the northern plains more conducive to pedestal crater formation, and explain why southern pedestal craters do not extend quite as close to the equator as those in the northern hemisphere.

[28] Although the necessity of ice-rich material has been the focus of this research, an important aspect of all pedestal crater formation models that has not been discussed in depth is that the impacts occur in fine-grained material [*Arvidson et al.*, 1976; *Barlow*, 2006; *McCauley*, 1973]. This element of the formation hypotheses may play an important role in the preferential formation of pedestal craters in the northern hemisphere. The resurfacing of the northern lowlands occurred via volcanic or sedimentary processes, and may have left a hundreds-of-meters-thick deposit overlying much of the northern terrain [*Head et al.*, 2002; *Clifford and Parker*, 2001; *Smith et al.*, 1999]. Researchers have suggested that the northern lowlands were once submerged under an extensive standing body of water. In this case, the flat northern topography could have resulted from subaqueous volcanism and deposition on the ocean floor [*Baker et al.*, 1991; *Parker et al.*, 1989]. Alternatively, early Hesperian volcanism may have been followed by fine-scale smoothing from the emplacement of outflow channel sediments [*Head et al.*, 2002]. The resulting smoothness has also been interpreted as fine-grained dust. This hypothesis is consistent with the low surface roughness and regional flatness derived from MOLA data [*Aharonson et al.*, 1998; *Christensen*, 1986; *Kreslavsky and Head*, 2000; *Smith et al.*, 1999].

[29] This low surface roughness has been specifically correlated to the Vastitas Borealis Formation, which covers most of the northern plains with a surface area of 1.8×10^7 km^2 [*Tanaka et al.*, 2005]. This region hosts an extremely high concentration of pedestal craters. The characteristic smoothness of the Vastitas Borealis Formation, suggests a composition of 100 m of sediment overlying volcanic ridged plains [*Kreslavsky and Head*, 2000, 2002; *Tanaka and Scott*, 1987]. Conversely, the southern hemisphere's Noachian terrain may be characterized by coarser material, yielding a much rougher surface, with higher local slopes. Although its ridged plains do form locally flat regions between craters, they are still extremely rough, as shown by interquartile-scale surface roughness calculations from MOLA profiles [*Smith et al.*, 1999]. Numerical granular flow models have shown the significant effects of surface roughness on ejecta emplacement and flow; rough surfaces and those with high friction coefficients between ejecta grains restrict ejecta mobility [*Wada and Barnouin-Jha*, 2006], and may be less conducive to armoring. It is thus likely that the southern hemisphere's terrain, having not been resurfaced by dust, sediment, or ash, is too rough and lacks the necessary fine-grained material to form large populations of pedestal craters. The northern hemisphere's younger, smoother deposits, which contain a much higher percentage of fine-grained material, provide a more appropriate setting for pedestal crater formation.

[30] Finally, the atmospheric and the fine-grained material factors may be working in conjunction with one another. It is possible that the concentration of fine-grained material in the northern hemisphere may enhance the dust content in its thicker atmosphere. A dustier atmosphere provides more nucleation sites for ice to form and precipitate, which could lead to preferential formation of the ice-rich deposit in the northern hemisphere.

[31] At this time, the relative impact of the atmosphere versus the target material in producing four times more pedestal craters between 0° and 60°N than between 0° and 60°S is not fully understood. Both factors, however, could contribute to the observed asymmetry in the hemispheric distribution of pedestal craters. Additional research is necessary to determine which, if either, is dominant.

4.6. Armoring Mechanism

[32] Several possible armoring agents have been suggested, including a coarse ejecta covering or lag deposit [e.g., *Arvidson et al.*, 1976], increased ejecta mobilization caused by volatile substrates [*Kieffer and Simonds*, 1980; *Stewart and Ahrens*, 2005; *Osinski*, 2006], glassy veneers from the distribution of impact melt [*Schultz and Mustard*, 2004], and/or an atmospheric blast/thermal effect [*Wrobel et al.*, 2006]. While our data show clear support for a sublimation-driven formation mechanism, they do not prove which of the above armoring mechanisms is correct. In this section, we offer a brief explanation of each method and discuss why, on the basis of our geomorphological analyses, we prefer the method proposed by *Wrobel et al.* [2006].

[33] The hypothesis that coarse material on the surface of the ejecta deposit prevents erosion of the ejecta [*Arvidson et al.*, 1976] applies only to the eolian deflation model, as winds are necessary to create the overlying lag deposit; it is thus not a control for the sublimation model of pedestal crater formation, although the permeability of the material on the pedestal surface likely has a significant impact on sublimation rates of volatiles within the pedestal. The production of proximal melts, including glassy impactites that armor the ejecta deposit is plausible [*Osinski*, 2006; *Schultz and Mustard*, 2004]. In this scenario, proximal melts are superimposed on the ice-rich material, forming a robust glassy covering that would prevent sublimation of near-surface ice. Another related working hypothesis is based on the theoretical prediction that dust can insulate ground ice for geologically long timescales [*Skorov et al.*, 2001; *Mellon et al.*, 1997]. This notion has been supported by empirical observations in the Antarctic Dry Valleys [*Marchant et al.*, 2002]. This armoring process involves impact into snow and/or ice overlying a fragmental silicate substrate. Impacts excavate to the fine-grained material below the layer of frozen volatiles. The fine-grained material is then mixed with some volatiles and distributed on top of the surrounding snow and/or ice. Even if some sublimation occurs in the upper layers of the ejecta deposit, the interspersed fine-grained material eventually reaches a critical thickness that sufficiently insulates the underlying frozen volatiles during periods of low obliquity [*Head et al.*, 2005; *Skorov et al.*, 2001]. While these armoring mechanisms may be capable of preserving volatiles underlying the pedestal crater surface, they seem inconsistent with our measurements of the physical attributes of pedestal craters; none explains why pedestals are anomalously large compared to their associated crater diameters, as confirmed by the high P/C ratio measurements, nor do they account for

minimal sinuosity of pedestal circumferences, as confirmed by the low Γ values.

[34] In the scenario proposed by *Wrobel et al.* [2006], the surface proximal to the impact becomes armored via an outwardly propagating atmospheric blast followed by a high-temperature thermal pulse. Studies suggest that atmospheric effects play a role both in the emplacement of ejecta, and on the modification of the terrain surrounding the impact site [e.g., *Barnouin-Jha and Schultz*, 1996; *Schultz*, 1992; *Schultz and Gault*, 1979]. *Wrobel et al.* [2006] note that the atmospheric blast would likely strip away any loose particulates, allowing the volatile-rich surface to be even more sensitive to the ensuing thermal pulse. Two possible armoring mechanisms could result from these atmospheric effects: (1) "...melting and migration of near-surface water may indurate soil by rapidly dissolving and precipitating salts...," or (2) "...the blast and thermal effects may combine to remove the volatile fraction, leaving behind a protective layer of fine, volatile-poor dust," [*Wrobel et al.*, 2006]. In either case, the sublimation rate from volatile-rich material composing the pedestal is reduced compared to the surrounding intercrater terrain upon return to low obliquity. It should be noted that because we are concerned only with sublimation (loss of volume due to removed ice) and not eolian deflation (loss of volume due to removed dust), it is irrelevant whether the ice in the volatile-rich target material was acting to cement the deposit. The only necessary aspect of the armored surface is to reduce the sublimation rate of volatiles from the pedestal material.

[35] *Wrobel et al.* [2006] calculate geotherms from the thermal response aspect of their model, after *Paterson* [1994]. These geotherms are shown for ice-rich and fine dust layers and are given on the basis of ambient Martian conditions as well as for conditions of increased temperature due to an engulfing hot vapor. On the basis of the geotherms, *Wrobel et al.* [2006] conclude that, "It is evident that lingering temperatures at ~30 s after the passage of the thermal pulse are high enough to produce a thermal wave extending to depths of several centimeters (temperatures above melting down to ~15 cm) at ~4 apparent crater diameters from impact of an ice-rich substrate. Consequently, if given enough time, temperatures will be sufficient to melt any ice present in the upper layers of a subsurface." The lateral extent of this heating is increased by considering the radiative effects of elevated temperatures higher in the atmosphere [*Rybakov et al.*, 1997]. By including these effects, significant heating can occur out to a distance of ~10 crater diameters [*Wrobel et al.*, 2006].

[36] The region closer to the impact (2–3 crater diameters) will of course be covered by the subsequent emplacement of ejecta. However, because pedestals extend to a distance much greater than the extent of the ejecta, we do not believe the ejecta plays a primary role in the armoring mechanism. Examples of pedestal craters where the extent of the ejecta is visible and entirely superposed on the farther-reaching pedestal have been identified (e.g., Figures 11b, 16b, 16d). It is likely, however, that ejecta deposits can protect the underlying material. Cases in which the ejecta is solely responsible for preserving the underlying volatile-rich layers have been observed and documented by *Black and Stewart* [2008]; these morphologies, known as excess ejecta craters, are distinct from pedestal craters, and are discussed in section 4.7.

[37] The method proposed by *Wrobel et al.* [2006] is thus capable of indurating the surface to a lateral extent of multiple crater radii and would preferentially yield circular pedestal craters due to the radially symmetric propagation of the atmospheric blast and thermal pulse. As such, we find this armoring mechanism to be consistent with our measurements. Our analyses do not, however, prove this armoring mechanism to be correct, and it is beyond the scope of this paper to provide a quantitative analysis or review of the atmospheric blast and thermal pulse. We hope that modelers will use the geomorphological constraints that we provide to test further the ability of each of the armoring mechanisms to indurate the surface and to inhibit sublimation of volatiles from the pedestals.

4.7. Related Morphologies

[38] Features similar to the pedestal craters discussed in this paper have been previously identified and associated with sublimation processes. These related morphologies share important traits with pedestal craters, but all differ from the strict definition of pedestal craters [*Barlow et al.*, 2000] in significant ways. *Meresse et al.* [2006] identified a population of "perched craters" in Acidalia and Utopia Planitia between 40°N and 70°N. These degraded features exhibit anomalously high ejecta volumes, in some cases exceeding the volume of the crater cavity. They are also characterized by often fluidized ejecta with low thermal inertia and infilling of the crater bowl. Although both perched craters and pedestal craters are elevated above the surrounding terrain, only perched craters display double-layer ejecta morphologies [*Barlow et al.*, 2000] and have distinctive, nearly constant depth versus diameter values [*Boyce et al.*, 2005]. *Meresse et al.* [2006] propose that these perched craters form via impact into an ice-rich target and subsequent resurfacing of the region. This resurfacing process includes the emplacement of fine-grained material over the ejecta deposits and significant infilling of the crater bowl, followed by erosional processes. Thermal erosion, consisting of weakening and disaggregation of the surface materials, preferentially affects the intercrater plains, which have a higher thermal inertia than the craters and ejecta deposits. The actual removal of the material begins with cryokarstic processes, including the sublimation of near-surface ice, followed by eolian deflation, lowering the elevation of the intercrater plains. The wind erosion continues to remove parts of the ejecta deposit as well, but the infilled crater cavity is largely resistant, leaving it perched [*Meresse et al.*, 2006].

[39] *Meresse et al.* [2006] note that, "perched craters have the same morphology as the type 3 craters described by *Boyce et al.*, (2005)..." *Boyce et al.* [2005] identified 414 of these type 3 craters, having a diameter range of 6 to 22.8 km, distinctly larger than the pedestal craters we measured. These type 3 craters, which were first described by *Garvin et al.* [2000], include all craters whose floor is at or above the elevation of the surrounding terrain, and are characterized by their remarkable shallowness and depth to diameter ratio [*Boyce et al.*, 2005]. The craters, which are generally found in the Vastitas Borealis Formation, have

floors which are typically ~0 to 250 m above the adjacent plains. *Boyce et al.* [2005] suggest that the distinctive depth to diameter ratios of these craters implies a unique erosional process that requires sublimation to have played a major role in their formation. This erosional style is unique to the Vastitas Borealis Formation on Mars, but is similar to a process that operates in high-latitude permafrost regions on Earth [*Boyce et al.*, 2005].

[40] The pedestal craters described here may have a similar formation mechanism to a population of fresh excess ejecta craters identified by *Black and Stewart* [2008], which are located primarily in Utopia Planitia between 32°N and 44°N. They identified 572 of these with a diameter range of 2.5 to 102 km. The volume of the ejecta material superposed on the preimpact surface is 2.5 to 5.8 times larger than the volume of the crater cavity. *Black and Stewart* [2008] argue that the excess volume cannot be explained by ejecta bulking alone, and therefore must be a secondary feature. They propose the following formation mechanism: Impact occurs into a rocky target overlain by an ice-rich layer(s) tens of meters thick. The ejecta deposit, which is a combination of rock and ice material, is distributed over the icy layer proximal to the crater cavity. Climate change causes the regional ice to sublimate, yielding a lag deposit, but the ejecta protects the underlying icy layer, prolonging the time over which is sublimates. Subsequent erosion of the intercrater lag layer deflates the surrounding surface. This lag deposit is preserved under the ejecta, producing the observed excess thickness of 20 to 100 m averaged over the continuous ejecta deposit. They conclude that the excess material may contain some of the original ice, but it could be purely a lag deposit [*Black and Stewart*, 2008]. The similarity between the formation mechanism they propose for excess ejecta craters and the mechanism we propose for pedestal craters suggests that these morphologies may be genetically related. This potential relation is strengthened by their excess thickness calculation (20 to 100 m), which mimics the range of pedestal heights we have measured at middle latitudes (~25 to 150 m).

[41] Morphologies also exist which are similar to the pits we have identified in association with pedestal craters. These related features can form via the sublimation of ice in numerous environments throughout the solar system [*Moore et al.*, 1996]. On Mars, these include dissected terrain [*Mustard et al.*, 2001; *Head et al.*, 2003], pits on the floors of craters [*Tornabene et al.*, 2007] and some outflow channels [*Levy and Head*, 2005], outwash plains and thermokarstic regions [*Costard and Kargel*, 1995], and formerly ice-rich and now beheaded pits in the proximal part of debris-covered glaciers [*Marchant and Head*, 2007]. For example, *Costard and Kargel* [1995] analyzed a similar pit morphology in western Utopia Planitia, just south of the population we have identified. These morphologically fresh, rimless pits occur in the surrounding substrate. They are interpreted to be due to sublimation and thermokarstic processes [*Costard and Kargel*, 1995; *Morgenstern et al.*, 2007; *Kargel and Costard*, 1993; *Soare et al.*, 2007]. Although they have similar characteristics and depths to pits in pedestal scarps, unlike pitted pedestal craters they reach depths below the elevation of the adjacent terrain. In particular, *Costard and Kargel* [1995] note that in Utopia Planitia, "...a few tens of rampart craters or other types of cratered mounds have annular moats around their edges." They argue that the moats have a thermokarstic origin, appearing similar to terrestrial fluvioglacial kettle lakes and alases [*Kargel and Costard*, 1993; *Costard and Kargel*, 1995]. In their model, "...impact meltwater infiltrated the permeable ejecta and then ponded or drained into rocks around the ejecta blanket. The infiltration of the water into the ground is possible because the impact would have thawed the surrounding ground. Under the cold climate of Mars, the drained water then froze, forming a concentration of segregated ice. During a warmer climate, the subsequent melting of this ice resulted in differential collapse and development of individual alases; slope retreat then resulted in a progressive widening of the thermokarst pits around the ejecta lobe. Finally, the coalescence of the alases produced a complete annular moat," [*Costard and Kargel*, 1995]. They also propose a mechanism in which the craters are not impact craters but mud volcanoes from geothermal liquefaction of frozen silts or slurries [*Costard and Kargel*, 1995].

[42] The pits in pedestal crater margins are also morphologically similar to scallops, which are found in both Utopia Planitia and Malea Planum in the plains between pitted pedestal craters [*Lefort et al.*, 2005, 2006, 2007; *Zanetti et al.*, 2008]. Scallops are thought to form via sublimation of interstitial ice from a volatile-rich mantling layer [*Howard*, 1978; *Lefort et al.*, 2006; *Zanetti et al.*, 2008]. These scallops are 5–20 m deep and can coalesce to form larger pits, much like the pits in the pedestal crater margins. They differ from pedestal crater pits, however, in a few important ways. First, the equator-facing slopes of scallops are generally shallower than their pole-facing slopes. Second, scallops are generally rounder in planform than pits around pedestal craters; scallops are not typically elongated in any given direction. Third, scallops can be considerably larger than pedestal crater pits, although this may be because pedestal crater pits are confined to the narrow pedestal crater scarp.

4.8. Formation Model and Implications for Ice Preserved under Pedestal Crater Surfaces

[43] On the basis of the evidence discussed throughout this paper, most notably the latitude dependence of pedestal craters, low Γ values and high P/C ratios, and the presence of marginal sublimation pits in some pedestal crater scarps, we favor an origin for pedestal craters based on sublimation of ice-rich deposits (Figure 17). Our model is as follows:

[44] 1. An impact occurs in a tens to hundreds-of-meters-thick, regional, middle-latitude layer of ice and snow, mixed with dust, which was deposited during a period of higher obliquity.

[45] 2. The impact distributes ejecta and impact melt around the crater rim, and triggers an atmospheric blast which is followed by a high-temperature thermal pulse [*Wrobel et al.*, 2006]. The strongest winds and hottest temperatures occur closest to the point of impact.

[46] 3. The surface proximal to the crater becomes indurated as a result of the impact process. This armored surface can extend to a distance of multiple crater radii, exceeding the lateral extent of the ejecta deposit. Because the effectiveness of the preferred armoring mechanism lessens moving radially away from the point of impact owing to weaker winds from the atmospheric blast and

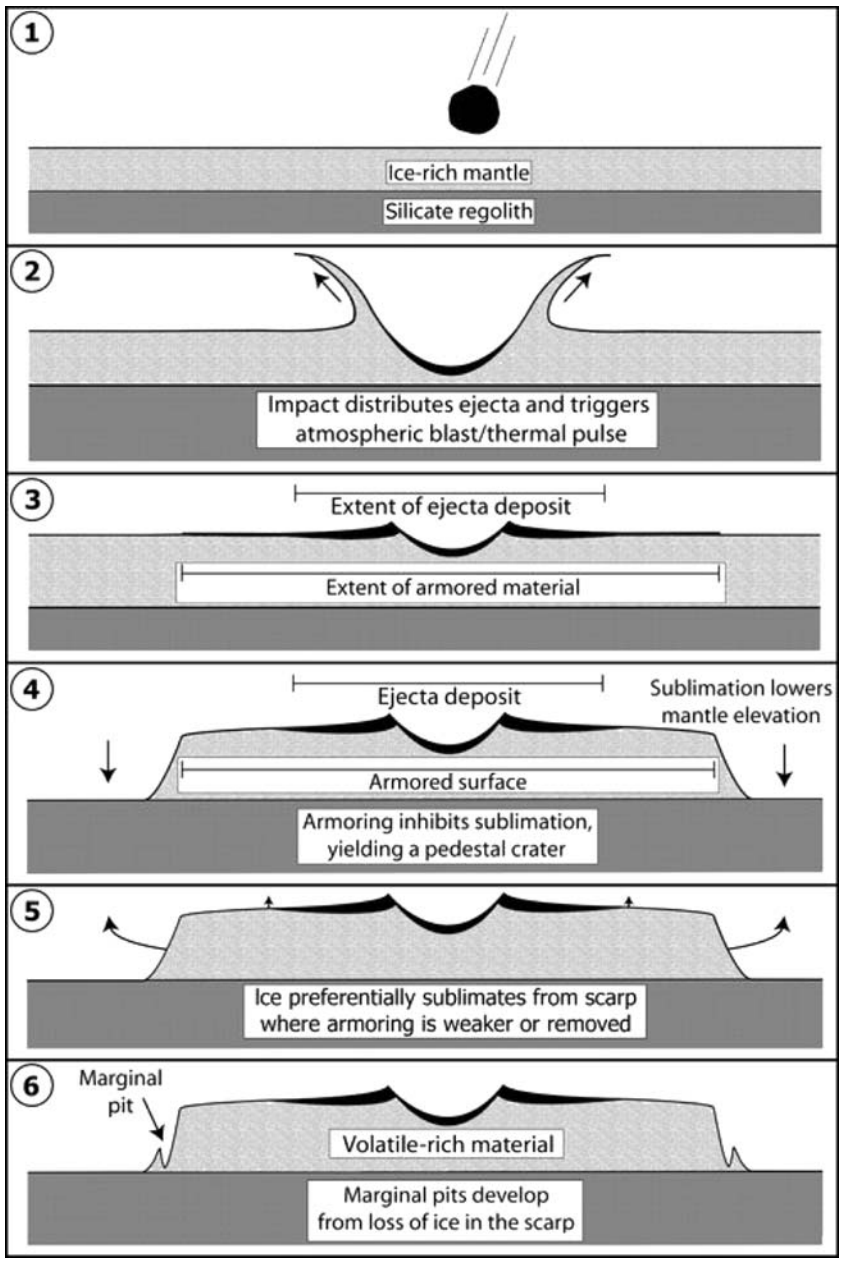

Figure 17. A schematic diagram showing the key steps in our conceptual model for the formation of pedestal craters. This sublimation-driven process is as follows: In step 1, an impact occurs into a volatile-rich deposit, overlying a fragmental silicate regolith. In step 2, the impact distributes ejecta and triggers an atmospheric blast followed by a high-temperature thermal pulse, desiccating and indurating the surface proximal to the impact. Step 3 shows that the extent of the armored material reaches beyond the margins of the ejecta deposit. In step 4, volatiles sublimate from the unarmored intercrater terrain during return to lower obliquity, lowering the elevation of the surrounding terrain, producing a scarp at the edge of the armored crater. Armoring inhibits sublimation from beneath the pedestal surface, resulting in a typical pedestal crater. In step 5, the scarps of taller pedestal craters, where the armoring has tapered off, receive enhanced insolation. Volatiles underlying the pedestal sublimate through the scarp at a faster rate than through the armored surface. In step 6, preferential sublimation of ice from the scarp produces marginal pits.

lower temperatures from the thermal pulse, we expect regions at the farthest extent of the pedestal to be weakly armored.

[47] 4. During return to low obliquity, climate change causes volatiles to sublimate from the unarmored intercrater terrain. The loss of volume lowers the elevation of the surrounding substrate, yielding a symmetrical, circular scarp at the edge of the armored crater. It is important to note that this process does not require eolian deflation which, due to predominant wind directions, would tend to reduce the

circularity of pedestals, in contrast to our observations. Armoring inhibits or slows sublimation from beneath the hardened pedestal surface, producing a typical pedestal crater, perched above a locally ice-rich substrate. Continued sublimation at the edge of the armored surface creates the debris-covered, marginal, pedestal scarps. The majority of pedestal craters reach an equilibrium between sublimation and debris cover, which stabilizes the margin of the pedestal.

[48] 5. Anomalously tall pedestal craters expose a larger surface area to insolation along their scarps. These higher, more extensive marginal slopes favor downslope movement and the thinning and shedding of any overlying protective regolith. As such, the slopes are preferentially mass wasted; volatiles within the pedestal material diffuse and sublimate through the scarp at a faster rate than through the armored surface. This effect may be enhanced by the tapering of the armor strength near the scarp, allowing for more rapid sublimation.

[49] 6. This sublimation process produces marginal pits, which appear to reach depths no greater than the vertical extent of the original ice-rich deposit, and do not extend to depths below the elevation of the intercrater, volatile-poor terrain [*Kadish et al.*, 2008]. Regions along the scarp where remnant armoring material inhibits sublimation yield localized preservation of the underlying substrate, producing the isolated mesas observed in some marginal pits.

[50] This sublimation-driven formation mechanism necessarily implies that pedestal craters represent the remnants of a formerly extensive ice/snow layer deposited during a period of higher obliquity. Depending on the age of specific pedestal craters and the rate of sublimation through the pedestal surface, it is likely that volatile-rich material is still preserved underneath many of the armored pedestal crater surfaces [*Kadish et al.*, 2008]. The population density and distribution of pedestal craters identified in this study (Figure 1) suggest that this ice-rich deposit persisted for a significant part of the recent past. For this to be the case, the obliquity of Mars must have been relatively higher than at present during parts of the Amazonian, which is consistent with models of past Martian obliquity [*Laskar et al.*, 2004].

5. Conclusions

[51] On the basis of the above findings, we draw the following conclusions about the nature of pedestal craters, and the implications they have for Martian climate change:

[52] 1. The distribution of 2696 pedestal craters identified in this study is nonrandom (Figures 1 and 2), occurring in the northern hemisphere almost exclusively poleward of 33°N, with the majority between 45° and 60°N latitude, where 60° represents the latitudinal poleward extent of our survey area. In the southern hemisphere they occur almost exclusively poleward of 40°S. This distribution is highly correlated with the distribution of ice-rich material predicted by climate models at higher obliquity [e.g., *Jakosky et al.*, 1995; *Richardson and Wilson*, 2002; *Mischna et al.*, 2003]. The pedestal crater population also mimics the distribution of a number of morphologies indicative of the presence of an ice-rich substrate at middle latitudes during periods of higher obliquity.

[53] 2. The consistently high P/C ratios, revealing that pedestals extend, on average, to a distance of >3 crater radii, and low Γ values, confirming the extreme circularity of the pedestals, support an armoring mechanism that can indurate the surface proximal to the impact to a distance greater than the extent of the ejecta, and that is radially symmetric. The necessity for a far-reaching armoring mechanism is further supported by examples of pedestal craters that have their ejecta deposits completely superposed on their respective pedestal surfaces. Although we have not proven any of the armoring mechanisms discussed in this paper, our geomorphological analyses are consistent with propagation of an impact-induced, symmetrical, atmospheric blast followed by a high-temperature thermal pulse [*Wrobel et al.*, 2006]. In this scenario, when an impact occurs into the ice-rich target material, the top few centimeters of the layer are desiccated and indurated, yielding the armored surfaces necessary to form anomalously large, circular pedestals via sublimation of volatiles from the intercrater terrain.

[54] 3. The generally small size range of pedestal craters suggests a delicate balance between crater size and the formation of this unique morphology; ejecta from larger craters may overwhelm the volatile substrate layer [*Barlow et al.*, 2001]. Volatiles buried beneath the ejecta of the larger craters may explain the anomalously high crater ejecta volumes observed in related crater morphologies [*Garvin et al.*, 2000; *Boyce et al.*, 2005; *Meresse et al.*, 2006; *Black and Stewart*, 2008].

[55] 4. Our observations strongly support a sublimation-driven formation mechanism for middle-latitude pedestal craters that does not require the role of eolian deflation, which in the past has been a critical aspect of hypotheses for pedestal crater formation. In our model, pedestal craters result from projectiles impacting into a target substrate consisting of a volatile-rich dust/snow/ice layer tens to hundreds of meters thick, overlying a dominantly fragmental silicate regolith. This material is deposited at middle latitudes during periods of higher obliquity. The proximal area becomes armored during the impact process. Climate change from a return to lower obliquity leads to sublimation and removal of the volatile-rich layer from the intercrater plains, which migrates poleward. This lowers the elevation of the regional terrain down to the underlying fragmental silicate-rich regolith, leaving generally circular pedestal craters elevated with armored surfaces overlying the preserved ice-rich material.

[56] 5. The characteristics of pedestal craters with pitted margins, interpreted to be sublimation pits, strongly support the current presence of volatiles below the armored surfaces of the pedestals [*Kadish et al.*, 2008].

[57] 6. These data and interpretations imply that during the Amazonian, significant climate change occurred. Examples of overlapping pedestal craters show that the deposition of decameters-thick, latitude-dependent, ice-rich layers has recurred numerous times. The armored surfaces of pedestal craters have therefore preserved a distinctive, accessible record of Amazonian climate history in the form of ice-rich, potentially layered deposits at the surface of Mars.

[58] We are currently (1) assessing regional variations in the properties of pedestal craters in order to understand the distribution of ancient volatile-rich layers [*Barlow and Perez*, 2003], (2) further analyzing the size-frequency dis-

tribution of pedestal craters to constrain the timing of these latitude-dependent volatile-rich layers, (3) targeting prominent pedestal craters with the SHARAD radar instrument [*Phillips et al.*, 2008] in order to test for the presence and structure of the proposed volatile-rich deposits, and (4) examining the relationships of these craters to related, sublimation-derived, crater morphologies to assess the links between pedestal formation and the production of perched craters and excess ejecta craters.

[59] **Acknowledgments.** Initial work on this topic by S.J.K. was supported by the NSF Research Experiences for Undergraduates program at Northern Arizona University (NSF award AST-0453611). We gratefully acknowledge financial support from the Mars Data Analysis Program (grants NNG04GJ99G and NNX07AN95G to J.W.H. and NAG512510 to N.G.B.), the Mars Fundamental Research Program (grant NNG05GM14G to N.G.B.), and the NASA Mars Express HRSC Guest Investigator Program (to J.W.H.).

References

Aharonson, O., M. T. Zuber, G. A. Neumann, and J. W. Head (1998), Mars: Northern hemisphere slopes and slope distributions, *Geophys. Res. Lett.*, *25*, 4413–4416, doi:10.1029/1998GL900057.

Arvidson, R. E., M. Coradini, A. Carusi, A. Coradini, M. Fulchignoni, C. Federico, R. Funiciello, and M. Salomone (1976), Latitudinal variation of wind erosion of crater ejecta deposits on Mars, *Icarus*, *27*, 503–516, doi:10.1016/0019-1035(76)90166-4.

Arvidson, R. E., E. Guinness, and S. Lee (1979), Differential aeolian redistribution rates on Mars, *Nature*, *278*, 533–535, doi:10.1038/278533a0.

Baker, V. R., R. G. Strom, V. C. Gulick, J. S. Kargel, G. Komatsu, and V. S. Kale (1991), Ancient oceans, ice sheets, and the hydrological cycles on Mars, *Nature*, *352*, 589–594, doi:10.1038/352589a0.

Barlow, N. G. (1993), Increased depth-diameter ratios in the Medusae Fossae Formation deposits of Mars, *Lunar Planet. Sci.* [CD-ROM], *XXIV*, 61–62.

Barlow, N. G. (1994), Sinuosity of Martian rampart ejecta deposits, *J. Geophys. Res.*, *99*, 10,927–10,935, doi:10.1029/94JE00636.

Barlow, N. G. (2004), Martian subsurface volatile concentrations as a function of time: Clues from layered ejecta craters, *Geophys. Res. Lett.*, *31*, L05703, doi:10.1029/2003GL019075.

Barlow, N. G. (2006), Impact craters in the northern hemisphere of Mars: Layered ejecta and central pit characteristics, *Meteorit. Planet. Sci.*, *41*, 1425–1436.

Barlow, N. G., and C. B. Perez (2003), Martian impact crater ejecta morphologies as indicators of the distribution of subsurface volatiles, *J. Geophys. Res.*, *108*(E8), 5085, doi:10.1029/2002JE002036.

Barlow, N. G., J. M. Boyce, F. M. Costard, R. A. Craddock, J. B. Garvin, S. E. H. Sakimoto, R. O. Kuzmin, D. J. Roddy, and L. A. Soderblom (2000), Standardizing the nomenclature of Martian impact crater ejecta morphologies, *J. Geophys. Res.*, *105*, 26,733–26,738, doi:10.1029/2000JE001258.

Barlow, N. G., J. Koroshetz, and J. M. Dohm (2001), Variations in the onset diameter for Martian layered Ejecta morphologies and their implications for subsurface volatile reservoirs, *Geophys. Res. Lett.*, *28*, 3095–3098, doi:10.1029/2000GL012804.

Barnouin-Jha, O. S., and P. H. Schultz (1996), Ejecta entrainment by impact-generating ring vorticies: Theory and experiments, *J. Geophys. Res.*, *101*, 21,099–21,115, doi:10.1029/96JE01949.

Barnouin-Jha, O. S., and P. H. Schultz (1998), Lobateness of impact ejecta deposits from atmospheric interactions, *J. Geophys. Res.*, *103*, 25,739–25,756, doi:10.1029/98JE02025.

Black, B. A., and S. T. Stewart (2008), Excess ejecta craters record episodic ice-rich layers at middle latitudes on Mars, *J. Geophys. Res.*, *113*, E02015, doi:10.1029/2007JE002888.

Boyce, J. M., P. Mouginis-Mark, and H. Garbeil (2005), Ancient oceans in the northern lowlands of Mars: Evidence from impact crater depth/diameter relationships, *J. Geophys. Res.*, *110*, E03008, doi:10.1029/2004JE002328.

Boynton, W. V., et al. (2002), Distribution of hydrogen in the near surface of Mars: Evidence for subsurface ice deposits, *Science*, *297*, 81–85, doi:10.1126/science.1073722.

Bradley, B. A., S. E. H. Sakimoto, H. Frey, and J. Zimbelman (2002), Medusae Fossae Formation: New perspectives from Mars Global Surveyor, *J. Geophys. Res.*, *107*(E8), 5058, doi:10.1029/2001JE001537.

Christensen, P. R. (1986), Regional dust deposits on Mars: Physical properties, age, and history, *J. Geophys. Res.*, *97*, 13,103–13,144.

Clifford, S. M., and T. J. Parker (2001), The evolution of the Martian hydrosphere: Implications for the fate of a primordial ocean and the current state of the northern plains, *Icarus*, *154*, 40–79, doi:10.1006/icar.2001.6671.

Costard, F. M. (1989), The spatial distribution of volatiles in the Martian hydrolithosphere, *Earth Moon Planets*, *45*, 265–290, doi:10.1007/BF00057747.

Costard, F. M., and J. S. Kargel (1995), Outwash plains and thermokarst on Mars, *Icarus*, *114*, 93–112, doi:10.1006/icar.1995.1046.

Fanale, F. P., J. R. Salvail, A. P. Zent, and S. E. Postawko (1986), Global distribution and migration of the subsurface ice on mars, *Icarus*, *67*, 1–18, doi:10.1016/0019-1035(86)90170-3.

Farmer, C. B., D. W. Davies, A. L. Holland, D. D. Laporte, and P. E. Doms (1977), Mars: Water vapor observations from the Viking orbiters, *J. Geophys. Res.*, *82*, 4225–4248, doi:10.1029/JS082i028p04225.

Fedorova, A., O. Korablev, J. Bertaux, A. Rodin, A. Kiselev, and S. Perrier (2006), Mars water vapor abundance from SPICAM IR spectrometer: Seasonal and geographic distributions, *J. Geophys. Res.*, *111*, E09S08, doi:10.1029/2006JE002695.

Feldman, W. C., et al. (2002), Global distribution of neutrons from Mars: Results from Mars Odyssey, *Science*, *297*, 75–78, doi:10.1126/science.1073541.

Feldman, W. C., J. W. Head, S. Maurice, T. H. Prettyman, R. C. Elphic, H. O. Funsten, D. J. Lawrence, R. L. Tokar, and D. T. Vaniman (2004a), Recharge mechanism of near-equatorial hydrogen on Mars: Atmospheric redistribution or sub-surface aquifer, *Geophys. Res. Lett.*, *31*, L18701, doi:10.1029/2004GL020661.

Feldman, W. C., et al. (2004b), Global distribution of near-surface hydrogen on Mars, *J. Geophys. Res.*, *109*, E09006, doi:10.1029/2003JE002160.

Feldman, W. C., et al. (2005), Topographic control of hydrogen deposits at low latitudes to midlatitudes of Mars, *J. Geophys. Res.*, *110*, E11009, doi:10.1029/2005JE002452.

Forget, F., F. Hourdin, R. Fournier, C. Hourdin, O. Talagrand, M. Collins, S. R. Lewis, P. L. Read, and J. Huot (1999), Improved general circulation models of the Martian atmosphere from the surface to above 80 km, *J. Geophys. Res.*, *104*, 24,155–24,176, doi:10.1029/1999JE001025.

Forget, F., R. M. Haberle, F. Montmessin, B. Levrard, and J. W. Head (2006), Formation of glaciers on Mars by atmospheric precipitation at high obliquity, *Science*, *311*, 368–371.

Garvin, J. B., S. E. H. Sakimoto, J. J. Frawley, and C. Schnetzler (2000), North polar region craterforms on Mars: Geometric characteristics from the Mars Orbiter Laser Altimeter, *Icarus*, *144*, 329–352, doi:10.1006/icar.1999.6298.

Greeley, R., R. O. Kuzmin, and R. M. Haberle (2001), Aeolian processes and their effects on understanding the chronology of Mars, *Space Sci. Rev.*, *96*, 393–404, doi:10.1023/A:1011917910624.

Grimm, R. E., and S. C. Solomon (1986), Tectonic tests of proposed polar wander paths for Mars and the Moon, *Icarus*, *65*, 110–121, doi:10.1016/0019-1035(86)90066-7.

Haberle, R. M., J. B. Pollack, J. R. Barnes, R. W. Zurek, C. B. Leovy, J. R. Murphy, H. Lee, and J. Schaeffer (1993), Mars atmospheric dynamics as simulated by the NASA Ames General Circulation Model: 1. The zonal-mean circulation, *J. Geophys. Res.*, *98*, 3093–3123, doi:10.1029/92JE02946.

Haberle, R. M., J. R. Murphy, and J. Schaeffer (2003), Orbital change experiments with a Mars general circulation model, *Icarus*, *161*, 66–89, doi:10.1016/S0019-1035(02)00017-9.

Hartmann, W. K. (1966), Martian cratering, *Icarus*, *5*, 565–576, doi:10.1016/0019-1035(66)90071-6.

Hartmann, W. K. (2005), Martian cratering 8: Isochron refinement and the chronology of Mars, *Icarus*, *174*, 294–320, doi:10.1016/j.icarus.2004.11.023.

Hartmann, W. K., and G. Neukum (2001), Cratering chronology and the evolution of Mars, *Space Sci. Rev.*, *96*, 165–194, doi:10.1023/A:1011945222010.

Head, J. W. (2000), Ancient polar deposits in the equatorial region of Mars: Tests using MOLA data, *Eos Trans. AGU*, *81*(19), Spring Meet. Suppl., Abstract P42A–10.

Head, J. W., and M. Kreslavsky (2004), Medusae Fossae Formation: Ice-rich airborne dust deposited during periods of high obliquity?, *Lunar Planet. Sci.* [CD-ROM], *XXXV*, Abstract 1635.

Head, J. W., and R. Roth (1976), Mars pedestal crater escarpments: Evidence for ejecta-related emplacement, in *Symposium on Planetary Cratering Mechanics*, *LPI Contrib.*, *259*, 50–52.

Head, J. W., M. A. Kreslavsky, and S. Pratt (2002), Northern lowlands of Mars: Evidence for widespread volcanic flooding and tectonic deformation in the Hesperian Period, *J. Geophys. Res.*, *107*(E1), 5003, doi:10.1029/2000JE001445.

Head, J. W., J. F. Mustard, M. A. Kreslavsky, R. E. Milliken, and D. R. Marchant (2003), Recent ice ages on Mars, *Nature*, *426*, 797–802, doi:10.1038/nature02114.

Head, J. W., et al. (2005), Tropical to mid-latitude snow and ice accumulation, flow and glaciation on Mars, *Nature*, *434*, 346–351, doi:10.1038/nature03359.

Howard, A. D. (1978), Origin of the stepped topography of the Martian poles, *Icarus*, *34*, 581–599, doi:10.1016/0019-1035(78)90047-7.

Hynek, B. M., R. J. Phillips, and R. E. Arvidson (2003), Explosive volcanism in the Tharsis region: Global evidence in the Martian geologic record, *J. Geophys. Res.*, *108*(E9), 5111, doi:10.1029/2003JE002062.

Jakosky, B. M. (1983), The role of seasonal reservoirs in the Mars water cycle: I. Seasonal exchange of water with the regolith, *Icarus*, *55*, 1–18, doi:10.1016/0019-1035(83)90046-5.

Jakosky, B. M., B. G. Henderson, and M. T. Mellon (1995), Chaotic obliquity and the nature of the Martian climate, *J. Geophys. Res.*, *100*, 1579–1584, doi:10.1029/94JE02801.

Kadish, S. J., and N. G. Barlow (2006), Pedestal crater distribution and implications for a new model of formation, *Lunar Planet. Sci.* [CD-ROM], *XXXVII*, Abstract 1254.

Kadish, S. J., J. W. Head, N. G. Barlow, and D. R. Marchant (2008), Martian pedestal craters: Marginal sublimation pits implicate a climate-related formation mechanism, *Geophys. Res. Lett.*, *35*, L16104, doi:10.1029/2008GL034990.

Kargel, J. S. (1986), Morphologic variations of Martian rampart crater ejecta and their dependencies and implications, *Lunar Planet. Sci.* [CD-ROM], *XVII*, Abstract 28.

Kargel, J. S., and F. M. Costard (1993), Possible occurrence and origin of massive ice in Utopia Planitia, in *Workshop on the Martian Northern Plains: Sedimentological, Periglacial, and Paleoclimatic Evolution*, pp. 7–8, Lunar Planet. Inst., Houston, Tex.

Kieffer, S. W., and C. H. Simonds (1980), The role of volailtes and lithology in the impact cratering process, *Rev. Geophys.*, *18*(1), 143–181, doi:10.1029/RG018i001p00143.

Kreslavsky, M. A., and J. W. Head (2000), Kilometer-scale roughness of Mars: Results from MOLA data analysis, *J. Geophys. Res.*, *105*, 26,695–26,712, doi:10.1029/2000JE001259.

Kreslavsky, M. A., and J. W. Head (2002), Fate of outflow channel effluents in the northern lowlands of Mars: The Vastitas Borealis Formation as a sublimation residue from frozen ponded bodies of water, *J. Geophys. Res.*, *107*(E12), 5121, doi:10.1029/2001JE001831.

Larson, S. K. (2007), The origins of four paterae of Malea Planum, Mars, M.S. thesis, 130 pp., Brigham Young Univ., Provo, Utah.

Laskar, J., A. C. M. Correia, M. Gastineau, F. Joutel, B. Levrard, and P. Robutel (2004), Long term evolution and chaotic diffusion of the insolation quantities of Mars, *Icarus*, *170*, 343–364, doi:10.1016/j.icarus.2004.04.005.

Lefort, A., P. Russell, and N. Thomas (2005), Ice sublimation landforms in Peneus and Amphitrites Patera, *Lunar Planet. Sci.* [CD-ROM], *XXXVI*, Abstract 1626.

Lefort, A., P. Russell, and N. Thomas (2006), Scallop-shaped depressions and mantle sublimation in the mid-latitudes of Mars, paper presented at Fourth Mars Polar Science Conference, Abstract 8061, Davos, Switzerland.

Lefort, A., P. Russell, N. Thomas, and the HiRISE Team (2007), Scalloped terrains in Utopia Planitia, insight from HiRISE, *Lunar Planet. Sci.* [CD-ROM], *XXXVIII*, Abstract 1796.

Levrard, B., F. Forget, F. Montmessin, and J. Laskar (2004), Recent ice-rich deposits formed at high latitudes on Mars by sublimation of unstable equatorial ice during low obliquity, *Nature*, *431*, 1072–1075, doi:10.1038/nature03055.

Levrard, B., F. Forget, F. Montmessin, and J. Laskar (2007), Recent formation and evolution of northern Martian polar layered deposits as inferred from a Global Climate Model, *J. Geophys. Res.*, *112*, E06012, doi:10.1029/2006JE002772.

Levy, J. S., and J. W. Head (2005), Evidence for remnants of ancient ice-rich deposits: Mangala Valles outflow channel, Mars, *Terra Nova*, *17*(6), 503–509, doi:10.1111/j.1365-3121.2005.00642.x.

Marchant, D. R., and J. W. Head (2007), Antarctic dry valleys: Microclimate zonation, variable geomorphic processes, and implications for assessing climate change on Mars, *Icarus*, *192*, 187–222, doi:10.1016/j.icarus.2007.06.018.

Marchant, D. R., A. R. Lewis, W. M. Phillips, E. J. Moore, R. A. Souchez, G. H. Denton, D. E. Sugden, N. Potter Jr., and G. P. Landis (2002), Formation of patterned ground and sublimation till over Miocene glacier ice in Beacon Valley, southern Victoria Land, Antarctica, *Geol. Soc. Am. Bull.*, *114*, 718–730, doi:10.1130/0016-7606(2002)114<0718:FOPGAS>2.0.CO;2.

McCauley, J. F. (1973), Mariner 9 evidence for wind erosion in the equatorial and midlatitude regions of Mars, *J. Geophys. Res.*, *78*, 4123–4137, doi:10.1029/JB078i020p04123.

Mellon, M. T., and B. M. Jakosky (1993), Geographic variations in the thermal and diffusive stability of ground ice on Mars, *J. Geophys. Res.*, *98*, 3345–3364, doi:10.1029/92JE02355.

Mellon, M. T., and B. M. Jakosky (1995), The distribution and behavior of Martian ground ice during past and present epochs, *J. Geophys. Res.*, *100*, 11,781–11,799, doi:10.1029/95JE01027.

Mellon, M. T., B. M. Jakosky, and S. E. Postawko (1997), The persistence of equatorial ground ice on Mars, *J. Geophys. Res.*, *102*, 19,357–19,369, doi:10.1029/97JE01346.

Mellon, M. T., W. C. Feldman, and T. H. Prettyman (2004), The presence and stability of ground ice in the southern hemisphere of Mars, *Icarus*, *169*, 324–340, doi:10.1016/j.icarus.2003.10.022.

Meresse, S., F. Costard, N. Mangold, D. Baratoux, and J. M. Boyce (2006), Martian perched craters and large ejecta volume: Evidence for episodes of deflation in the northern lowlands, *Meteorit. Planet. Sci.*, *41*, 1647–1658.

Mischna, M. A., and M. I. Richardson (2005), A reanalysis of water abundances in the Martian atmosphere at high obliquity, *Geophys. Res. Lett.*, *32*, L03201, doi:10.1029/2004GL021865.

Mischna, M. A., M. I. Richardson, R. J. Wilson, and D. J. McCleese (2003), On the orbital forcing of Martian water and CO_2 cycles: A general circulation model study with simplified volatile schemes, *J. Geophys. Res.*, *108*(E6), 5062, doi:10.1029/2003JE002051.

Mitrofanov, I., et al. (2002), Maps of subsurface hydrogen from the high energy neutron detector, Mars Odyssey, *Science*, *297*, 78–81, doi:10.1126/science.1073616.

Moore, J. M., M. T. Mellon, and A. P. Zent (1996), Mass wasting and ground collapse in terrains of volatile-rich deposits as a solar system-wide geological process: The pre-Galileo view, *Icarus*, *122*, 63–78, doi:10.1006/icar.1996.0109.

Morgenstern, A., E. Hauber, D. Reiss, S. van Gasselt, G. Grosse, and L. Schirrmeister (2007), Deposition and degradation of a volatile-rich layer in Utopia Planitia and implications for climate history on Mars, *J. Geophys. Res.*, *112*, E06010, doi:10.1029/2006JE002869.

Mouginis-Mark, P. (1979), Martian fluidized crater morphology: Variations with crater size, latitude, altitude, and target material, *J. Geophys. Res.*, *84*, 8011–8022, doi:10.1029/JB084iB14p08011.

Mouginis-Mark, P. (1987), Water or ice in the Martian regolith? Clues from rampart craters seen at very high resolution, *Icarus*, *71*, 268–286, doi:10.1016/0019-1035(87)90152-7.

Mustard, J. F., C. D. Cooper, and M. K. Rifkin (2001), Evidence for recent climate change on Mars from the identification of youthful near-surface ground ice, *Nature*, *412*, 411–414, doi:10.1038/35086515.

Mutch, P., and A. Woronow (1980), Martian rampart and pedestal craters' ejecta-emplacement: Coprates quadrangle, *Icarus*, *41*, 259–268, doi:10.1016/0019-1035(80)90009-3.

Neukum, G., B. A. Ivanov, and W. K. Hartmann (2001), Cratering records in the inner solar system in relation to the Lunar reference system, in *Chronology and Evolution of Mars*, edited by R. Kallenbach et al., pp. 87–104, Int. Space Sci. Inst., Bern.

Osinski, G. R. (2006), Effect of volatiles and target lithology on the generation and emplacement of impact crater fill and ejecta deposits on Mars, *Meteorit. Planet. Sci.*, *41*, 1571–1586.

Parker, T. J., R. S. Saunders, and D. M. Schneeberger (1989), Transitional morphology in West Deuteronilus Mensae, Mars: Implications for modification of the lowland/upland boundary, *Icarus*, *82*, 111–145, doi:10.1016/0019-1035(89)90027-4.

Paterson, W. B. (1994), *The Physics of Glaciers*, 3rd ed., 250 pp., Pergamon, New York.

Phillips, R. J., et al. (2008), Mars north polar deposits: Stratigraphy, age, and geodynamical response, *Science*, *320*, 1182–1185, doi:10.1126/science.1157546.

Richardson, M. I., and R. J. Wilson (2002), Investigation of the nature and stability of the Martian seasonal water cycle with a general circulation model, *J. Geophys. Res.*, *107*(E5), 5031, doi:10.1029/2001JE001536.

Rybakov, V. A., I. V. Nemtchinov, V. V. Shuvalov, V. I. Artemiev, and S. A. Medveduk (1997), Mobilization of dust on the Mars surface by the impact of small cosmic bodies, *J. Geophys. Res.*, *102*, 9211–9220, doi:10.1029/96JE03569.

Schultz, P. H. (1992), Atmospheric effects on ejecta emplacement, *J. Geophys. Res.*, *97*, 11,623–11,662, doi:10.1029/92JE00613.

Schultz, P. H., and D. E. Gault (1979), Atmospheric effects on Martian ejecta emplacement, *J. Geophys. Res.*, *84*, 7669–7687.

Schultz, P. H., and A. B. Lutz (1988), Polar wandering of Mars, *Icarus*, *73*, 91–141, doi:10.1016/0019-1035(88)90087-5.

Schultz, P. H., and J. F. Mustard (2004), Impact melts and glasses on Mars, *J. Geophys. Res.*, *109*, E01001, doi:10.1029/2002JE002025.

Scott, D. H., and K. L. Tanaka (1982), Ignimbrites of Amazonis Planitia region of Mars, *J. Geophys. Res.*, *87*, 1179–1190, doi:10.1029/JB087iB02p01179.

Skorov, Y. V., W. J. Markiewicz, A. T. Basilevsky, and H. U. Keller (2001), Stability of water ice under a porous nonvolatile layer: Implications to the south polar layered deposits of Mars, *Planet. Space Sci.*, *49*, 59–63, doi:10.1016/S0032-0633(00)00121-5.

Smith, D. E., et al. (1999), The global topography of Mars and implications for surface evolution, *Science*, *284*, 1495–1503, doi:10.1126/science.284.5419.1495.

Smith, M. D. (2002), The annual cycle of water vapor on Mars as observed by the Thermal Emission Spectrometer, *J. Geophys. Res.*, *107*(E11), 5115, doi:10.1029/2001JE001522.

Smith, M. D. (2004), Interannual variability in TES atmospheric observations of Mars during 1999–2003, *Icarus*, *167*, 148–165, doi:10.1016/j.icarus.2003.09.010.

Soare, R. J., J. S. Kargel, G. R. Osinski, and F. M. Costard (2007), Thermokarst processes and the origin of crater-rim gullies in Utopia and western Elysium Planitia, *Icarus*, *191*, 95–112, doi:10.1016/j.icarus.2007.04.018.

Sprague, A. L., D. M. Hunten, L. R. Doose, R. E. Hill, W. V. Boynton, M. D. Smith, and J. C. Pearl (2006), Mars atmospheric water vapor abundance: 1991–1999, emphasis 1998–1999, *Icarus*, *184*, 372–400, doi:10.1016/j.icarus.2006.05.021.

Stewart, S. T., and T. J. Ahrens (2005), Shock properties of H_2O ice, *J. Geophys. Res.*, *110*, E03005, doi:10.1029/2004JE002305.

Tanaka, K. L. (2000), Dust and ice deposition in the Martian geologic record, *Icarus*, *144*, 254–266, doi:10.1006/icar.1999.6297.

Tanaka, K. L. (2005), Geology and insolation-driven climatic history of Amazonian north polar materials on Mars, *Nature*, *437*, 991–994, doi:10.1038/nature04065.

Tanaka, K. L., and D. H. Scott (1987), Geologic map of the polar regions of Mars, *U.S. Geol. Surv. Misc. Invest. Ser. Map I-1802-C*.

Tanaka, K. L., J. A. Skinner Jr., T. M. Hare, T. Joyal, and A. Wenker (2003), Resurfacing history of the northern plains of Mars based on geologic mapping of Mars Global Surveyor data, *J. Geophys. Res.*, *108*(E4), 8043, doi:10.1029/2002JE001908.

Tanaka, K. L., J. A. Skinner Jr., and T. M. Hare (2005), Geologic map of the northern plains of Mars, *U.S. Geol. Surv. Sci. Invest. Ser.*, *Map 2888*.

Tornabene, L. L., A. S. McEwen, G. R. Osinski, P. J. Mouginis-Mark, J. M. Boyce, R. M. E. Williams, J. J. Wray, and J. A. Grant (2007), Impact melting and the role of subsurface volatiles: Implications for the formation of valley networks and phyllosilicate-rich lithologies on early Mars, in *Seventh International Conference on Mars, July 9–13, 2007, Pasadena CA* [CD-ROM], *LPI Contrib.*, *1353*, Abstract 3288.

Touma, J., and J. Wisdom (1993), The chaotic obliquity of the planets, *Science*, *259*, 1294–1297, doi:10.1126/science.259.5099.1294.

Wada, K., and O. Barnouin-Jha (2006), The formation of fluidized ejecta on Mars by granular flows, *Meteorit. Planet. Sci.*, *41*, 1551–1569.

Watters, T. R., et al. (2007), Radar sounding of the Medusae Fossae Formation Mars: Equatorial ice or dry, low-density deposits?, *Science*, *318*, 1125–1128, doi:10.1126/science.1148112.

Wrobel, K., P. H. Schultz, and D. Crawford (2006), An atmospheric blast/thermal model for the formation of high-latitude pedestal craters, *Meteorit. Planet. Sci.*, *41*, 1539–1550.

Zanetti, M., H. Hiesinger, D. Reiss, E. Hauber, and G. Neukum (2008), Scalloped depressions in Malea Planum, southern Hellas Basin, Mars, *Lunar Planet. Sci.* [CD-ROM], *XXXIX*, Abstract 1682.

N. G. Barlow, Department of Physics and Astronomy, Northern Arizona University, Flagstaff, AZ 86011, USA.

J. W. Head and S. J. Kadish, Department of Geological Sciences, Brown University, Providence, RI 02912, USA.